The Molecular Code for Hemoglobin Allostery Revealed by Linking the Thermodynamics and Kinetics of Quaternary Structural Change. 1. Microstate Linear Free Energy Relations†

Robert A. Goldbeck,*,‡ Raymond M. Esquerra,§ Jo M. Holt,|| Gary K. Ackers,|| and David S. Kliger‡

Department of Chemistry and Biochemistry, University of California, Santa Cruz, California 95064, Department of Chemistry and Biochemistry, San Francisco State University, San Francisco, California 94132, and Department of Biochemistry and Molecular Biophysics, Washington University School of Medicine, St. Louis, Missouri 63110

Received March 29, 2004; Revised Manuscript Received June 18, 2004

ABSTRACT: A novel model linking the thermodynamics and kinetics of hemoglobin's allosteric (R → T) and ligand binding reactions is applied to photolysis data for human HbCO. To describe hemoglobin's kinetics at the microscopic level of structural transitions and ligand-binding events for individual [*ij*]-ligation microstates (^{ij}R → ^{ij}T, ^{ij}R + CO → $^{(i+1)k}$R, and ^{ij}T + CO → $^{(i+1)k}$T), the model calculates activation energies, $^{ij}\Delta G^{\ddagger}$, from previously measured cooperative free energies of the equilibrium microstates (Huang, Y., and Ackers, G. K. (1996) *Biochemistry 35*, 704−718) by using linear free energy relations ($^{ij}\Delta G^{\ddagger} - {}^{01}\Delta G^{\ddagger} = \alpha[{}^{ij}\Delta G - {}^{01}\Delta G]$, where the parameter α, describing the variation of activation energy with reaction energy perturbation, can depend on the natures of both the reaction and the perturbation). The α value measured here for the allosteric dynamics, 0.21 ± 0.03, corresponds closely to values observed previously, strongly suggesting that the thermodynamic microstate energies directly underlie the allosteric kinetics (as opposed to the α($^{ij}\Delta G_{RT}$) serving merely as arbitrary fitting parameters). Besides systematizing the study of hemoglobin kinetics, the utility of the microstate linear free energy model lies in the ability to test microscopic aspects of allosteric dynamics such as the "symmetry rule" for quaternary change deduced previously from thermodynamic evidence (Ackers, G. K., et al. (1992) *Science 255*, 54−63). Reflecting a remarkably detailed correspondence between thermodynamics and kinetics, we find that a kinetic model that includes the large free energy splitting between doubly ligated T microstates implied by the symmetry rule fits the data significantly better than one that does not.

The cooperative ligand binding mechanism of hemoglobin remains incompletely understood despite extensive studies motivated both by its important role in respiration and its usefulness as a model for the allosteric regulation of protein function. The difficulty in studying hemoglobin's mechanism lies in the nature of cooperativity itself, which tends to obscure the properties of reaction intermediates. Typically too ephemeral for equilibrium studies and commingled in kinetic studies, it is the properties of just such intermediates that can illuminate most strongly the mechanism of cooperativity.

Progress has been made recently in measuring the free energies of all 10 equilibrium ligation microstates (the two end states, T_0 and R_4, and eight intermediate states) for a variety of ligation systems (*1*). Those thermodynamic results point to an allosteric mechanism that lies between the traditional limiting cases of a pure two-state model (MWC)[1] (*2*) and a purely sequential model (KNF) (*3*). In this mechanism, the equilibrium between the two canonical quaternary states, R and T, of the hemoglobin tetramer is modulated by strain forces induced within its constituent αβ-chain dimers by the binding of ligands to the T structure. The strain energies are observed to be localized in large part to a given dimer, a situation that is sometimes called dimer autonomy (*4*). Moreover, most of the strain energy is produced by the binding of the first ligand to a given (T-state) dimer, the binding of the second ligand being observed to have a much smaller effect (sequential cooperativity). Those thermodynamic observations underlie a "symmetry rule" for quaternary change: the binding of at least one ligand to each dimer is necessary to switch the tetramer from the (low affinity) T to the (high affinity) R state (and is sufficient in the absence of allosteric effectors). Note that this symmetry requirement for the R state, the presence of ligands on each dimer, is different in nature than the symmetry proposed in the early MWC model. The latter postulated a strict conformational symmetry between subunits throughout an R- or T-state tetramer that has not been borne out by observation. Overall, the symmetry rule model of

† Supported by the National Institute of General Medical Sciences (NIH) grant GM38549.

* To whom correspondence should be addressed. Tel.: 831-459-4007. Fax: 831-459-2935. E-mail: goldbeck@chemistry.ucsc.edu.

‡ University of California.

§ San Francisco State University.

|| Washington University School of Medicine.

[1] Abbreviations: IHP, inositol hexaphosphate; DPG, 2,3-diphosphoglycerate; LFER, linear free energy relation; MLFER, microstate linear free energy relation; TLFER, two-state linear free energy relation; Tris, tris(hydroxymethyl)aminomethane; EDTA, ethylenediamine-tetraacetic acid; MWC, Monod, Wyman, and Changeux; KNF, Koshland, Nemethy, and Filmer.

10.1021/bi049393v CCC: $27.50
Published on Web 08/28/2004

hemoglobin cooperativity can be considered a hierarchical combination of the KNF and MWC models in that the sequential cooperativity of ligand binding observed within each dimer is coupled to the two-state quaternary equilibrium mediating the global cooperativity of the tetramer.

We now report that the detailed knowledge of ligation-intermediate thermodynamic properties underpinning this hierarchical model of hemoglobin allostery also provides a key to understanding its dynamics. We find that the free energies of the intermediates provide a simple guide to understanding the kinetics of hemoglobin allostery in the face of the complexity that comes with its cooperative nature. In doing so, we are able to independently test important predictions of the thermodynamic model, including the symmetry rule.

In favorable cases, the thermodynamic and kinetic effects of perturbing a reaction are linked such that the activation energy $\Delta G^{\ddagger}$ changes in a way that can be predicted simply from the change in the reaction energy. The simplest example of this situation is a linear free energy relation: $\Delta G^{\ddagger} = \alpha(\Delta G - \Delta G_0) + \Delta G_0^{\ddagger}$, where ΔG_0 and $\Delta G_0^{\ddagger}$ refer to the unperturbed reaction and $0 \leq \alpha \leq 1$ (*5*). A transition state for which α is small is sometimes called "reactant like" with respect to perturbation, meaning that its free energy is perturbed in a manner very similar to that of the reactant, whereas a transition state for which α is closer to one would be called "product like". In the case of the R→T quaternary structural transition of hemoglobin, the activation energy appears to obey a linear free energy relation with an α value of 0.2 for a variety of perturbations such as pH, ligand binding, and anionic allosteric effectors (*6*). In other words, the R→T transition state is rather R-like with respect to perturbation by the common physiological effectors.

Kinetic modeling of the R→T transition after ligand photolysis is typically complicated by the fact that concurrent ligand rebinding modulates the allosteric rate constant. Because the hemoglobin tetramer cooperatively binds a total of four ligands, the observed R→T dynamics reflects the aggregate behavior of an evolving distribution of ligation intermediates, rather than a single rate constant $k_{R_i \rightarrow T_i}$ corresponding to a particular number *i* of ligands bound (*7*). Previous models have attempted to simplify this situation by assuming that the rate constant decreases by a constant factor *d* with the binding of each additional ligand (i.e., $k_{R_i \rightarrow T_i} = k_{R_0 \rightarrow T_0}/d^i$) (*8*). With respect to linear free energy relationships, this is equivalent to assuming a constant change in the free energy difference between R and T conformations as each ligand binds, an approximation that has proven useful in analyzing the kinetics of hemoglobin allostery (*7*).

With the more complete information about allosteric energies now available (*9*), it has become possible to construct more precise microscopic linear free energy kinetic models. In the model presented here, free energies of reaction for the microscopic allosteric transitions, ${}^{ij}\Delta G_{R \rightarrow T}$, were used with a linear free energy relation to predict relationships between the corresponding free energies of activation, ${}^{ij}\Delta G^{\ddagger}_{R \rightarrow T}$, where [*ij*] labels the ligation microstates, *i* indicating the number of ligands and *j* labeling their distribution among the α and β heme sites within each dimer (using the numbering convention shown in Table 1). The reaction free energies were derived from the cooperative free energies measured previously for all 10 equilibrium ligation microstates of HbCO by Huang and Ackers (*9*). In addition, a second free energy relation was used to predict similar relationships between the activation energies of the ligand binding reactions for the R and T microstates, again using the cooperative free energies as inputs for calculating the reaction free energies of the microstates. Thus, the cooperative free energies served here to both link thermodynamically the microstate linear free energy relations (MLFERs) of ligand binding and quaternary structure change and to systematize the microscopic kinetics of each process.

Table 1: HbCO Microstate Thermodynamic Parameters (0.1 M Cl^-)[a]

Species[b]	[*ij*]	${}^{ij}\Delta G_c$[c]	Equilibrium conformation	${}^{ij}K_{RT}$[d]
	[01]	0	T	5×10^4
	[11]	3.3 ± 0.2	T	2×10^2
	[12]	3.4 ± 0.3	T	2×10^2
	[21]	4.2 ± 0.3	T	50
	[22]	6.5 ± 0.3	R	0.1
	[23]	6.6 ± 0.3	R	0.1
	[24]	6.5 ± 0.3	R	0.1
	[31]	6.5 ± 0.3	R	8×10^{-3}
	[32]	6.6 ± 0.2	R	8×10^{-3}
	[41]	6.3 ± 0.1	R	4×10^{-4}

[a] Free energies are in kcal/mole. [b] Tetrameric Fe/FeCO ligation species. Orientation of α and β subunits are indicated in species [01]. Open squares represent unliganded Fe subunits and X-filled squares represent liganded subunits. [c] Data of Huang and Ackers (*9*). [d] Calculated from ${}^{ij}K_{RT} = \exp\{-[{}^{ij}\Delta G_c(T) - {}^{ij}\Delta G_c(R)]/RT\}$ and the ΔG_c values in Figure 2.

In extending our understanding of the allosteric dynamics of photolyzed HbCO to the microscopic level of individual ligation microstates, an important issue addressed by the MLFER model is the symmetry rule for quaternary change inferred previously from purely thermodynamic evidence. The model is applied in the present work to photolysis data for HbCO, and to data for iron−cobalt HbCO hybrids in a companion paper (*10*), to assess what role the symmetry rule may also play in the dynamics of hemoglobin allostery.

EXPERIMENTAL PROCEDURES

Time-resolved absorption spectra were measured in the Soret spectral region (400−460 nm) at 65 logarithmically spaced delay times that ranged from 16 ns to 40 ms after CO photolysis by use of an optical multichannel analyzer apparatus described previously (*11*). The HbCO samples were photolyzed with 20-mJ pulses of 532-nm light from a frequency-doubled Nd:YAG laser with a pulse length of 10 ns. Photoselection effects were eliminated by orienting the laser and probe polarizations at the magic angle, 54.7°. The photolysis difference spectrum reported for each delay time

Scheme 1

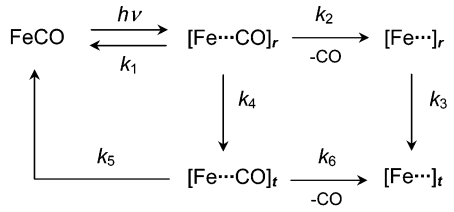

represents the average of 1000 individual absorption measurements using a 15-ns sampling gate. The HbCO concentration was 120 μM in a sealed 0.5-mm path length anaerobic cell. Before sealing under 1 atm CO in a glovebag, the samples were degassed under argon, followed by CO, and reduced with excess dithionite (250 μM). Each sealed sample was used for 48−128 individual absorption measurements at all 65 delay times. There was no discernible difference in the static absorption spectra of samples measured before and after the laser photolysis protocol, which excluded the possibility that permanent photodegradation of the sample may have affected our results. Sample temperature was maintained at 20 ± 1 °C. Samples contained Hb A that had been column-stripped of the physiological allosteric effector DPG. Effector-bound samples were produced from stripped Hb A by adding 2 mM IHP. All samples were in pH 7.4 buffered solutions containing 0.1 M Tris, 0.1 M NaCl, and 1 mM EDTA.

Kinetic Modeling Procedures

Geminate Recombination. The earliest ligand recombination processes in photolyzed HbCO involve the geminate recombination of ligands that have not yet escaped from the protein matrix. Geminate recombination appears to proceed in two kinetic phases, the first with a time constant on the order of tens of nanoseconds (*12*−*14*), and the second with a longer time constant observed to be ∼160 ns in double-pulse photolysis experiments (*15*). The geminate recombination processes are overlapped in time by a relaxation of protein tertiary structure at the heme pocket (*16*).

Geminate rebinding to heme iron and ligand escape from the heme pocket into solution were represented (Scheme 1) by the first-order rate constants k_1 and k_2, respectively, for the fast recombination process and by k_5 and k_6, respectively, for the slow process. Tertiary relaxation from the liganded heme conformation (*r*), present in HbCO before photolysis, to the unliganded form (*t*) after photolysis was represented by the rate constants k_3 and k_4. These relaxation rate constants were set equal to one another on the assumption that structural relaxation drives the modulation of geminate binding and escape kinetics implied by the two rebinding rate processes, while the reverse coupling is weak (i.e., the tertiary dynamics are not themselves affected by the presence or absence in the heme pocket of geminately dissociated ligand).

Thus, photolysis of the Fe−CO bond produces a geminately dissociated species $[Fe\cdots CO]_r$ whose evolution branches between three processes: (1) recombination through k_1, (2) ligand escape through k_2 to produce a CO-less heme pocket that eventually relaxes to $[Fe\cdots]_t$, and (3) structural relaxation to $[Fe\cdots CO]_t$, which in turn branches between rebinding and ligand escape to reach the final geminate product, $[Fe\cdots]_t$. The overall probability p for photodissociation of Fe−CO to produce $[Fe\cdots]_t$ in Scheme 1 (geminate escape yield) is given by

$$p = (k_2 + k_4k_6/(k_5 + k_6))/(k_1 + k_2 + k_4) \qquad (1)$$

Scheme 1 contains five independent rate constants (after setting $k_3 = k_4$) corresponding to three possible observed time constants. (Although, note that only two time constants, τ_1 and τ_2, are typically detected on the geminate recombination time scale in model-independent 6-exponential global analyses of HbCO photolysis data (*17*).) We thus used three free parameters, $g_1 = (k_1 + k_2 + k_4)^{-1}$, $g_2 = (k_5 + k_6)^{-1}$, and $g_3 = k_4^{-1}$, to represent the three microscopic geminate time constants.

Two additional constraints were needed to determine the six geminate rates: (1) the value of p was set to 0.7, and (2) the ratio of the yields of the fast and slow geminate recombination processes was set to 0.67, the experimental values observed by Esquerra et al. (*15*) under essentially identical excitation conditions. The length and intensity of the photolysis laser pulse used in these experiments tended to produce significant rephotolysis of geminately recombined sample, which lowered the observed geminate recombination yield from the literature value, ∼40%. However, rephotolysis was not explicitly incorporated into the model used here. In this light, the value of p served as an effective photolysis yield intended to allow Scheme 1 to approximate the results of more elaborate possible models convoluting the kinetics of Scheme 1 with the effects of strong excitation over a finite time period corresponding to the time profile of the laser pulse. We also tested the assumption that $p = 0.7$ by fitting the photolysis data to a model that included p as a free parameter and the constraint that tertiary relaxation had a minimal effect on the photolysis difference spectral intensities of the *r* and *t* species (i.e., $R_r = R_t$) using the heme spectral-type labels introduced below. Those fits returned values of p that were very close to 0.7. In any event, the optimized values of parameters obtained from fitting procedures in which p was fixed were relatively insensitive to variations in p over the range ±7%. In applying this kinetic scheme to analyzing the data, the geminate species were treated on a per heme basis, as the geminate dynamics for each heme in the tetramer are expected to be independent of one another (*18*).

Bimolecular Recombination and Allostery. We attempted with the model presented in Scheme 2 to analyze the kinetics of ligand binding and quaternary structure change in photolyzed HbCO at the microscopic level of individual conformational microstates, paralleling the equilibrium thermodynamic analysis of Huang and Ackers (*9*).

An overview of the allosteric kinetics can be summarized phenomenologically in terms of the four longest observed time constants obtained in a 6-exponential global fit of the Soret absorption data (*17*). The first of these, $\tau_3 \sim 1$ μs, has been assigned to heme pocket tertiary relaxation concomitant with a relaxation of dimer−dimer contacts at the $\alpha_1\beta_2$ interface, the latter constituting the first step in a compound mechanism for the quaternary transition (*19*−*22*). The structural changes associated with this relaxation are probably rather subtle, involving changes in dimer-dimer contacts at the hinge region of the interface such as formation of a

Scheme 2

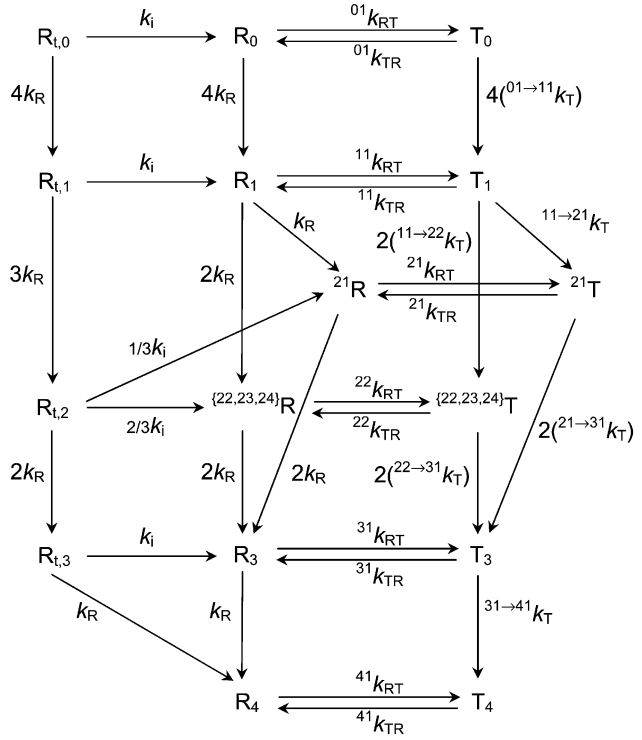

Trp$\beta_2$37-Asp$\alpha_1$94 hydrogen bond rather than the large relative motion of subunits associated with the full R→T transition (*22*). Correspondingly, the amplitude of the spectral changes observed in the heme bands are very small (*17*). The next time constant (τ_4), on the order of tens of microseconds, is conventionally assigned to the R→T quaternary structural transition (*8*). However, the quaternary nature of the process associated with τ_3 implies that τ_4 is more precisely associated with the rate-limiting step of the R→T pathway. Moreover, kinetic competition between structural relaxation from the R state and bimolecular ligand recombination typically convolutes microscopic rate constants for the R→T transition and CO recombination together in τ_4. Finally, $\tau_5 \approx 200$ μs and $\tau_6 \approx 4$ ms are traditionally assigned as time constants for the fast and slow bimolecular recombination of CO to the R- and T-state conformations of the protein, respectively.

The right-hand rectangle of allosteric reactions in Scheme 2 bears some resemblance to a simple two-state scheme (Figure 1). However, anticipating the correlation between allosteric kinetics and the pattern of microstate cooperative energies presented below, Scheme 2 explicitly distinguished the special character of the ^{21}T conformational microstates from the other doubly liganded T-microstates, ^{2j}T (where $j = 2, 3, 4$). As discussed further below, the different cooperative energies of the two "flavors" of T_2 microstates leads to a branching (shown offset to the right) from the rectangle of traditional allosteric reactions. (For simplicity, the singly and triply ligated microstates were grouped by ligation number and quaternary conformation as in more traditional kinetic schemes, e.g., $R_1 = \{^{11}R,^{12}R\}$.) This bifurcation of kinetics among the doubly liganded microstates is the central novel feature of the model. It has the significant consequence of introducing two distinct R→T rate constants for the doubly liganded states, $^{21}k_{RT}$ and $^{2j}k_{RT}$.

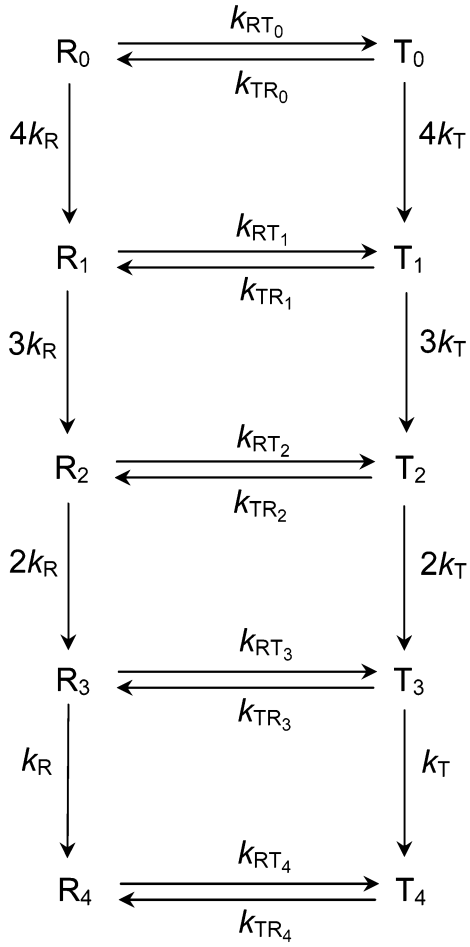

FIGURE 1: Simple two-state model of cooperativity during bimolecular rebinding of ligands to photolyzed HbCO. Traditional two-state models postulate that ligand binding affinities and rate constants depend only on the quaternary state, R or T, the R-state CO rebinding rate constant, k_R, being an order of magnitude faster than that for T, k_T (statistical factors multiply these rate constants by the number of heme sites available for binding in the tetramer). The number of ligands bound, *n*, then affects observed binding affinities and rate constants (cooperativity) only by shifting the R → T equilibria $L_n = [T_n]/[R_n] = k_{RTn}/k_{TRn} = L_0c^n$, where $L_0 \approx 10^4$, in equal increments corresponding to the factor $c \approx 0.01$. The two-state model does not distinguish between conformational microstates of a given *n* value. Thus, the distinction between ^{21}T and the other T_2 microstates, important in the symmetry rule model, is absent in the traditional two-state model (see Table 1 for microstate indexing).

Although some of the allosteric rate constants considered in Scheme 2 are expected to be negligibly small (e.g., $^{01}k_{TR}$), most of the twelve rate processes shown are expected to make a significant contribution to the observed time constant τ_4. A deconvolution of the individual contributions of the microstate rate constants was accomplished with the MLFER model described below. All of the allosteric rates were determined in this model by using two free parameters, $^{01}k_{RT}$ and the MLFER parameter α_{RT}.

The two-state rate constant for bimolecular recombination of CO to the R microstates, k_R, was a free parameter in the model and is expected to have a value similar to the inverse of the observed time constant τ_5. (All bimolecular rate processes were treated in the kinetic modeling as pseudo-first order.) Similarly, a two-state rate constant for T-state bimolecular recombination, k_T, would be expected to have a value $\sim\tau_6^{-1}$. However, another novel feature of the model presented here is the introduction of different bimolecular

CO recombination rate constants for different T ligation states (e.g., the rate constant for recombination to a heme in the T_0 state $^{01\rightarrow 11}k_T$ in Scheme 2, is not equal to that for T_3, $^{31\rightarrow 41}k_T$). Reflecting the bifurcation of kinetics at the T_2 microstate level mentioned above, the model also distinguishes the reaction of CO with the T_1 microstates to form ^{21}T ($^{11\rightarrow 21}k_T$) from the reaction forming the remaining $^{2,j\neq 1}T$ microstates (e.g., $^{11\rightarrow 22}k_T$), and similarly for the reactions of ^{21}T and $^{2,j\neq 1}T$ to produce T_3. This feature of the model was included as a further consequence of the different steps in the cooperative energies (free energy penalties) upon ligand binding of microstates within the T state (*9*), which by thermodynamic linkage imply different binding affinities. The different affinities in turn imply different binding rates via linear free energy relations. The width of the distribution about the central value (expected to be near the two-state value) of the T-state rate constants resulting from the MLFER model then becomes of interest and is discussed below. As in the case of the allosteric structure relaxation, all of the bimolecular ligand binding rate constants (for both R and T microstates) were determined by using two free parameters, k_R and the MLFER parameter α_{CO}.

The R_t species in Scheme 2 ($R_{t,0}$, $R_{t,1}$ ...) correspond to the various ways in which the geminate product of Scheme 1, $[Fe\cdots]_t$, can be produced within a given photolyzed tetramer after geminate recombination has restored an Fe−CO bond to 30% of the hemes on average for all of the tetramers. In other words, $R_{t,0}$ corresponds to a tetramer with all four hemes photolyzed to the $[Fe\cdots]_t$ form, $R_{t,1}$ corresponds to three hemes photolyzed to $[Fe\cdots]_t$, and so on. Besides bimolecular recombination with CO which is not expected to be very extensive during the short lifetime of R_t, the $R_{t,n}$ species also undergo interfacial relaxation via k_i (corresponding to the inverse of the observed time constant τ_3) to produce the corresponding R_n species. We thus set $k_i = \tau_3^{-1}$ in the kinetic model. (Because the relaxation corresponding to k_i is detected only very weakly in Soret absorption data, we did not attempt to investigate the possibility that this rate constant may also depend on the tetramer's ligation state in a manner analogous to k_{RT}.) The factors of 1/3 and 2/3 in the branching of $R_{t,2}$ to produce ^{21}R and $^{\{22,23,24\}}R$, respectively, are statistical factors reflecting the relative probabilities of forming each species.

Scheme 1, which is posed on a per heme basis, must be combined with Scheme 2, which is necessarily posed on a per tetramer basis because of heme−heme interactions, to obtain an overall kinetic model for photolyzed HbCO. While one could describe the geminate recombinations on the same per tetramer basis as used in Scheme 2, this would lead to a cumbersome proliferation of possible intermediates as the various steps in Scheme 1 proceed at the four hemes. The observation that the distribution of heme ligation among the tetramers produced by geminate recombination is well predicted by simple combinatorial statistics (*23*) implies that these reactions proceed identically, as well as independently, within each heme site. This finding (and the large difference in the time scales of the geminate and the later processes) simplifies the task of connecting Schemes 1 and 2, since one can then use binomial statistics and the probability p of a CO ligand being bound to a particular heme site to calculate the distribution of the geminate-escape heme product $[Fe\cdots]_t$ among the corresponding tetrameric species, $R_{t,n}$. The details of this procedure are presented in the Appendix.

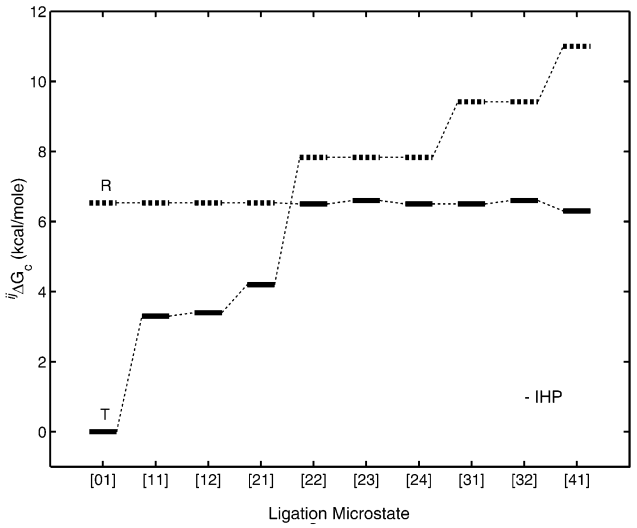

FIGURE 2: Scheme of cooperative energies, $^{ij}\Delta G_c$, for ^{ij}R and ^{ij}T microstates of (stripped) HbCO. Experimental values (solid) were taken from data of Huang and Ackers (*9*). Remaining values (dashed) used as fixed inputs for MLFER kinetic model were estimated as discussed in text.

Microstate Linear Free Energy Model. The MLFER model used the free energies of quaternary structure transformation and ligand binding reactions (Scheme 2) to predict relationships between the activation energies of those reactions for individual R and T conformational microstates. In the case of the $^{ij}R\rightarrow{}^{ij}T$ structural relaxations, reaction free energies were calculated from thermodynamic data for the cooperative free energies using the relation

$$^{ij}\Delta G_{RT} = {}^{ij}\Delta G_c(T) - {}^{ij}\Delta G_c(R) \qquad (2)$$

The cooperative energies used for stripped and IHP-bound hemoglobin are shown in Figures 2 and 3, respectively. Not all of the cooperative energies shown were measured directly (experimental values of Huang and Ackers (*9*) for stripped HbCO are shown as solid lines), equilibrium experiments generally being limited to observing either the R or T quaternary form of a given ligation microstate, whichever form is lowest in energy. Therefore, further assumptions were required to arrive at estimates for the remaining values (dashed lines).

To estimate the remaining values for the R microstates, we assumed that the R configurations not observed by Huang and Ackers (^{01}R, ^{11}R,^{12}R, and ^{21}R) had $^{ij}\Delta G_c$ values equal to those measured for the R species that were observed (^{22}R, ^{23}R,^{24}R,^{31}R,^{32}R, and ^{41}R). In other words, we assumed that all the ^{ij}R had approximately the same $^{ij}\Delta G_c$ value, ~6.5 kcal/mol in HbA_0 (the notable exception being ^{41}R, which is stabilized by 0.3 kcal/mol relative to the other R microstates by addition of the fourth ligand, a phenomenon called quaternary enhancement). This extrapolation of the near-ligation-independence of the R-state energies observed by Huang and Ackers to the unobserved R microstates seems reasonable, given that the dimer−dimer forces underlying changes in cooperative energies upon ligand binding are much weaker in the R microstates than in the T microstates. Moreover, the value of $L_0 \equiv [T_0]/[R_0]$ implied by $^{01}\Delta G_{RT} =$

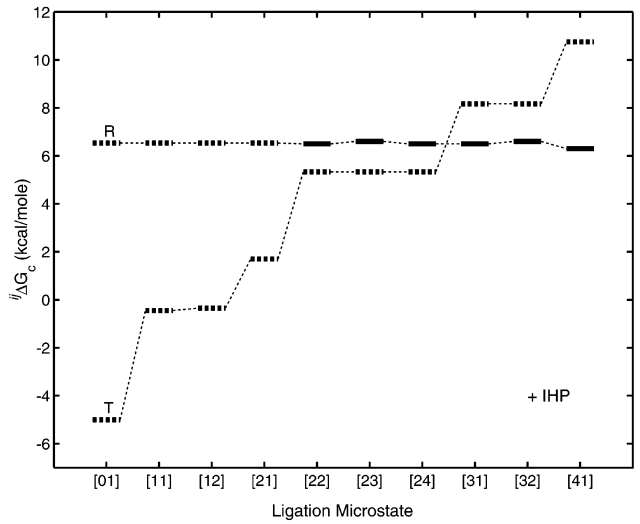

FIGURE 3: Scheme of ^{ij}R and ^{ij}T cooperative energies, $^{ij}\Delta G_c$, used as inputs for MLFER kinetic model of HbCO + IHP. Line types are as in Figure 2 legend. For simplicity, the zero of cooperative energy used in the IHP-free case was adjusted by the energy of IHP binding to R_4, so that the effect of IHP binding appears only as a lowering of the T-state energies by the preferential binding energy.

$^{01}\Delta G_c(T) - {}^{01}\Delta G_c(R) = 6.5$ kcal/mol (cf. $^{01}K_{RT}$, Table 1) is in reasonable agreement with experimental values measured under similar conditions (*24*).

We estimated similarly the energy of the rightmost T microstate in Figure 2, $^{41}\Delta G_c(T)$, from an experimental value of $c = 0.01$ in the two-state allostery expression $L_4 = [T_4]/[R_4] = c^4 L_0$ (cf. $^{41}K_{RT}$, Table 1), a procedure which yielded a value of 11 kcal/mol (*25*). The value of $^{ij}\Delta G_c(T)$ for the [22], [23], and [24] ligation microstates was determined to be 7.9 ± 0.3 kcal/mol from measurements of L_2 in di-(Fe→Co) substituted Hb tetramers, the results of which are presented in a companion paper (*10*). Finally, completion of the cooperative energies shown in Figure 2 requires the value of $^{ij}\Delta G_c$ for ^{31}T and ^{32}T. In the absence of further experimental guidance, this was assumed to be halfway intermediate between the values for the $^{\{22,23,24\}}$T and ^{41}T conformational microstates. (Note that the kinetic model is expected to be least sensitive to the $^{ij}\Delta G_c$ values of the ^{31}T, ^{32}T, and ^{41}T microstates as their populations are expected to remain relatively small during the post-photolysis ligand recombination reactions.)

It is well-known that the allosteric effector IHP binds more strongly to the deoxy T state than to the liganded R state (*24*). To model the effect of IHP on HbCO photolysis kinetics, however, information is required on the effect of IHP binding on the energies of individual T microstates corresponding to ligation intermediates (see Figure 3). Although comprehensive equilibrium measurements of microstate energies such as those reported by Huang and Ackers (*9*) have not been carried out for IHP-bound Hb, the effect of IHP binding on the energies of some intermediate ligation states has been investigated by Robert et al. (*26*). Their results, along with similar results for DPG binding (*27*), suggest that the magnitude of the preferential binding energy of organic phosphate effectors to the T quaternary structure relative to the R structure decreases monotonically to zero with increasing oxygen ligation. We thus modeled the effect of preferential IHP binding on the energies of the T-microstate ligation intermediates as a linear function of the number of CO molecules bound to the tetramer. The free energy of preferential IHP-deoxyHb binding, $^{01}\Delta G_{IHP}$, was set to the value obtained from a linear least-squares fit to free energies calculated from equilibrium constants (λ_0, λ_1, λ_2, and λ_4) reported by Robert et al. (*26*), −5.0 kcal/mol.

Relative R→T allosteric activation energies, and thus rate constants, were then calculated from

$$^{ij}\Delta G^{\ddagger}_{RT} = \alpha_{RT}(^{ij}\Delta G_{RT} - {}^{01}\Delta G_{RT}) + {}^{01}\Delta G^{\ddagger}_{RT} \quad (3)$$

where the linear free energy parameter α_{RT} was determined by optimizing the fit of the MLFER model to the kinetic data. For a given value of α_{RT}, this approach fixed the values of the microscopic R→T rate constants $^{ij}k_{RT}$ obtained from an Arrhenius expression to within a common factor ($^{01}k_{RT}$), which was also optimized as a parameter in the model. Thus,

$$^{ij}k_{RT} = {}^{01}k_{RT} \exp\{-\alpha_{RT}(^{ij}\Delta G_{RT} - {}^{01}\Delta G_{RT})/RT\} \quad (4)$$

where R is the gas constant and T is temperature.

Rate constants for the microstate bimolecular recombination reactions were calculated similarly from the microstate cooperative free energies by use of a linear free energy relation and the free parameters α_{CO} and k_R. The activation free energies of the bimolecular recombination reactions are related to the reaction free energies by

$$^{ij\rightarrow(i+1)k}\Delta G^{\ddagger}_{CO} = \alpha_{CO}[^{ij\rightarrow(i+1)k}\Delta G_{CO} - {}^{01\rightarrow11}\Delta G_{CO}(R)] + {}^{01\rightarrow11}\Delta G^{\ddagger}_{CO}(R) \quad (5)$$

where (ij) and $((i + 1)k)$ index the reactant and product microstates, respectively, and the reference reaction is ^{01}R + CO → ^{11}R. The free energies of ligand binding and cooperativity are linked for the process ^{ij}T + CO → $^{(i+1)k}$T such that

$$^{ij\rightarrow(i+1)k}\Delta G_{CO} = {}^{(i+1)k}\Delta G_c(T) - {}^{ij}\Delta G_c(T) + {}^{D}\Delta G_{CO} \quad (6)$$

where $^{D}\Delta G_{CO}$ is the free energy of (noncooperative) ligand binding to free $\alpha\beta$-chain dimers. Equation 6 refers only to T states, because the relative ligation-independence of R-microstate cooperative energies mentioned above implies that the R microstates have identical ligand affinities ($^{ij\rightarrow(i+1)k}\Delta G_{CO}(R) = {}^{D}\Delta G_{CO}$) and, hence, rate constants, k_R. In the approximation that the R microstates have identical cooperative energies, Equations 5 and 6 lead to the following relationship between the T and R rates:

$$^{ij\rightarrow(i+1)k}k_T = k_R \exp(-\alpha_{CO}(^{(i+1)k}\Delta G_c(T) - {}^{ij}\Delta G_c(T))/RT) \quad (7)$$

The values of the two free parameters in this relation, k_R and α_{CO}, were determined by optimization of the fit of the model to the data, paralleling the approach to modeling of the allosteric rates represented by eq 4.

To summarize the MLFER model parametrization, seven parameters were optimized simultaneously in the fitting of the model to the data: the geminate time constant parameters introduced above, g_1, g_2, and g_3; and the allosteric parameters $^{01}k_{RT}$, α_{RT}, k_R, and α_{CO}. However, an additional free

Table 2: Fitting Parameter Values for MLFER Model of Photolyzed HbCO Kinetics[a]

parameter	trial[d]	optimized	averaged[e]
g_1[b]	0.02	0.01	
g_2[b]	0.12	0.13	
g_3[b]	0.05	0.05	
α_{RT}	0.2	0.20	0.21 ± 0.03
$^{01}k_{RT}$	2×10^4	1.6×10^4	$1.6 \pm 0.4 \times 10^4$
α_{CO}	0.5	0.44	0.45 ± 0.03
k_R[c]	5×10^3	9.6×10^3	$1.0 \pm 0.3 \times 10^4$

[a] Rate constants are in s^{-1}. [b] Time constants are in μs. [c] Pseudo-first-order rate constant (1 mM CO). [d] Trial values used to determine the starting point for optimization procedures. [e] Statistical average of $N = 100$ optimizations run using $^{ij}\Delta G_c$ and ΔG_{IHP} energy inputs that were randomly varied by $\pm$ 0.3 kcal (standard deviation) from values given in text.

parameter introduced above as an input to the MLFER model, τ_3, was first optimized in a global fit of a model-independent 6-exponential decay expression to the data. Taken altogether, then, the MLFER model presented here used eight parameters to describe the full time course of ligand rebinding and structural relaxation in photolyzed HbCO. The values of these parameters, with the constraint conditions described above, were sufficient to algebraically determine the values of the rate constants in Schemes 1 and 2.

Dimer-Tetramer and Effector Binding Equilibria. The model accounted for the multiple equilibria corresponding to the dissociation of carboxy R tetramers into dimers (eq 8) and the binding of IHP to the R_4 and dimer species (eqs 9 and 10) in the prephotolysis sample. (Photolysis-induced changes in dimerization and effector binding were neglected, as these were expected to occur too slowly to significantly influence hemoglobin allostery on the time scales investigated here.) The free energy value for the dissociation of the sample (R_4) into dimers ($\Delta G_D = -RT \cdot \ln(K_D) = -8.0$ kcal/mol), taken from Huang and Ackers (*9*), corresponded to 10% dissociation on a per heme basis under the conditions in this study. The value of the free energy of IHP binding to the R_4 tetramer species (-5 kcal/mol) was estimated from the data of Robert et al. (*26*), and the IHP binding energy for the dimer was estimated from the data of Gray (*28*) to be about 1 kcal/mol less stable than that for the R tetramer ($\Delta G_{IHP}{}^D \approx \Delta G_{IHP}{}^R + 1$ kcal/mol).

$$R_4 \overset{K_D}{\rightleftharpoons} 2D_2 \tag{8}$$

$$R_4 + IHP \overset{K_{IHP}^R}{\rightleftharpoons} R_4 \cdot IHP \tag{9}$$

$$D_2 + IHP \overset{K_{IHP}^D}{\rightleftharpoons} D_2 \cdot IHP \tag{10}$$

(Note that D_2 in the above equations refers to a doubly CO-ligated dimer.)

Parameter Optimization. Typical trial starting values for the parameters are shown in Table 2. Most of these were obtained from the observed time constants as explained above (e.g., $^{01}k_{RT} \sim \tau_4{}^{-1}$) or in the literature (e.g., α_{RT}) (*6*). The trial value for the CO binding linear free energy parameter was obtained from the relation $\alpha_{CO} \approx (\log(k_R) - \log(k_T))/(\log(K_{CO}(R)) - \log(K_{CO}(T)))$ and previously measured values for the (two-state) binding rate constants and equilibrium constants (*29*). The mathematical procedures used to optimize the model parameters are described in the Appendix.

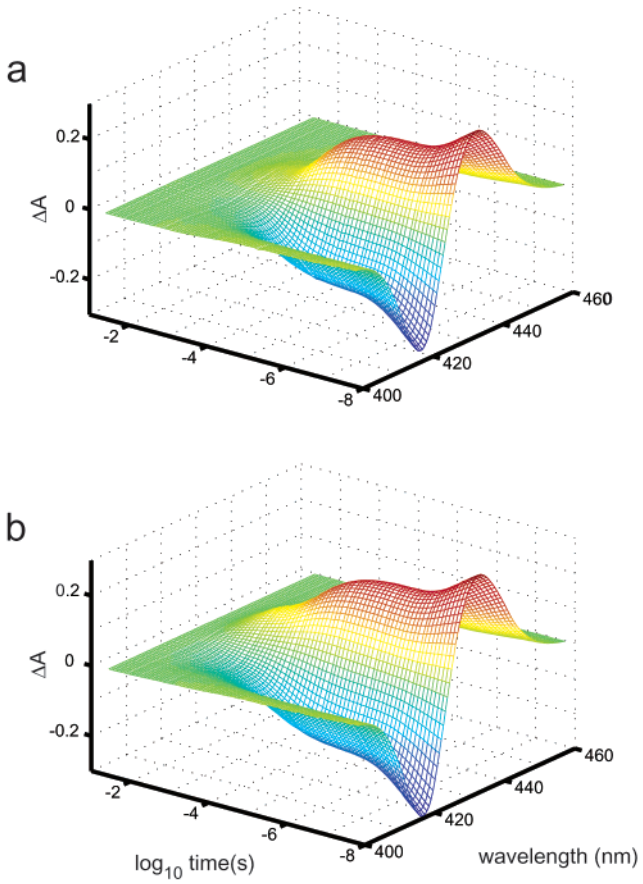

FIGURE 4: Time-resolved Soret region absorption spectra of photolyzed HbCO. Photolysis difference spectra for (a) HbCO stripped of DPG and (b) HbCO plus IHP.

RESULTS

The MLFER model was tested with HbCO photolysis data measured under two allosteric conditions: (1) protein "stripped" of the physiological organic phosphate effector DPG (Figure 4a), and (2) in the presence of 2mM IHP (Figure 4b), an allosteric effector strongly stabilizing the deoxy T state relative to the liganded R state. The addition of IHP lengthened the time required for ligand to recombine bimolecularly after photodissociation, as can be seen by comparing time-resolved photolysis difference absorption spectra for HbCO with and without IHP. More dramatic effects of IHP on bimolecular recombination have been reported by previous workers using different conditions of pH, temperature, or incomplete photodissociation (*30*, *31*). The difference was most evident here in the 1−10 ms time regime, wherein recombination to T-state hemoglobin is expected to be the dominant process. This effect can be seen more clearly in the SVD components (Figures 5 and 6). The first component is an approximate measure of the extent of heme photodissociation, its spectrum (see Figures 5a and 6a) resembling the static Hb − HbCO difference spectrum. The corresponding temporal amplitudes thus approximately reflect the time course of ligand rebinding, both geminate and bimolecular. The latter process was extended in time by the large increase in the T-state recombination amplitude in the presence of IHP (see Figures 5d and 6d). The second SVD

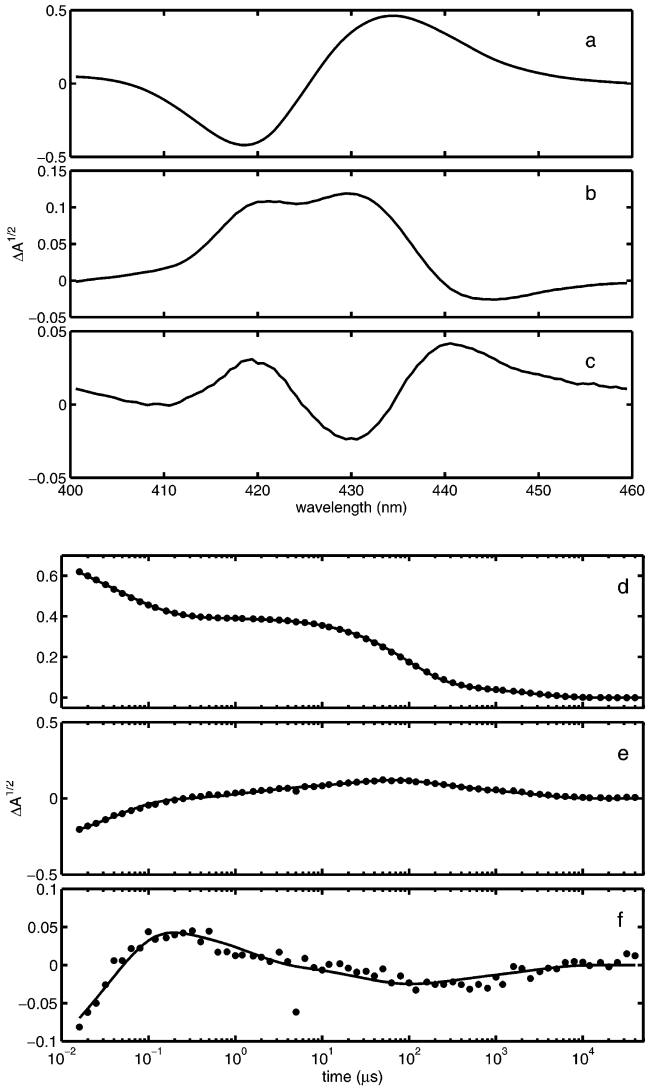

FIGURE 5: The first three SVD components of photolysis data for stripped HbCO. (a−c) Basis spectra (columns of $\mathbf{U} \cdot \mathbf{S}^{1/2}$). (d−f) Temporal amplitudes (columns of $\mathbf{V} \cdot \mathbf{S}^{1/2}$) shown as points. Lines represent fits of the SVD temporal amplitudes calculated from the MLFER kinetic model.

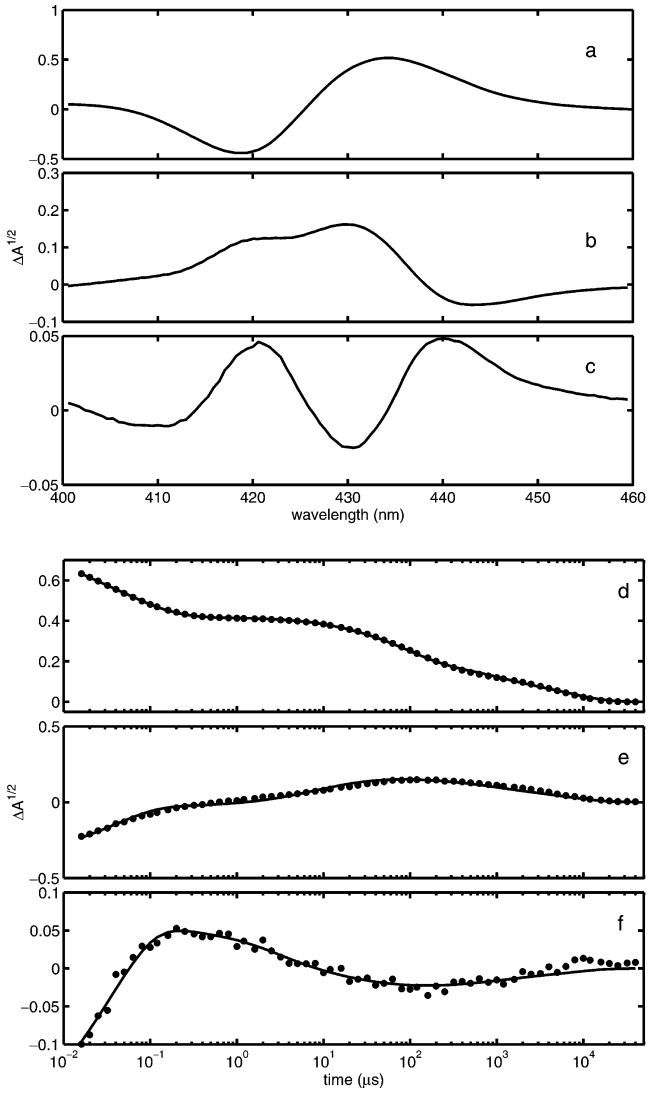

FIGURE 6: The first three SVD components of photolysis data for HbCO + IHP. Panels are labeled as in Figure 5 legend.

component corresponds approximately to the extent of heme spectral relaxation, which is apparent as an increasingly blue-shifted deoxy peak as the protein structure relaxes at the heme pocket. The magnitude of spectral relaxation was larger in the presence of IHP (compare Figures 5b and 6b), again suggesting an increased R→T rate constant and increased T-state production. The correlation of T-state stabilization and faster R→T kinetics apparently induced here by IHP would be an expected consequence of the linear free energy relation known to link the thermodynamics and kinetics of allostery in response to many types of perturbations. The exploration of this linkage on a microstate level is the program of the MLFER model evaluated below.

A more quantitative picture of the effect of IHP on post-photolysis kinetics is provided by the results of simple 6-exponential fits to the data. These fits show significant changes in the last three observed processes (Figure 7). (The assignments of the observed time constants and corresponding decay spectra to specific molecular processes are given above.) The amplitude of the T-state recombination more than doubles, whereas the R-state recombination amplitude decreases by 30% (Table 3). The amplitude of the fourth process also changes, decreasing by ∼15%, although τ_4 does not change. These changes are consistent with increased T state production in the presence of IHP and a concomitant decrease in the amount of R states recombining with CO. Although an increase in the R→T conversion rate might also be expected to decrease the magnitude of τ_4, this effect was apparently offset by a decrease in the CO recombination rates, which are also convoluted into this time constant. The decreased contribution of recombination to the fourth process in the presence of IHP was also reflected in a decrease in observed amplitude, the intrinsic spectral amplitude of the R→T process being much smaller than that of ligand recombination. Accordingly, the 437-nm band in the fourth decay spectrum (see Figure 7), the shape of which is a convolution of the CO difference spectrum (cf. decay spectrum of process 5), and the R−T difference spectrum (similar in band shape to the decay spectrum of process 3), shifted to longer wavelength by 1 nm on the addition of IHP.

The phenomenological picture provided by the 6-exponential fits shows that binding of IHP to the tetramer directly reduces the CO binding rate constant of hemoglobin, particularly when the tetramer is in its T conformation. The observed time constants assigned to bimolecular recombina-

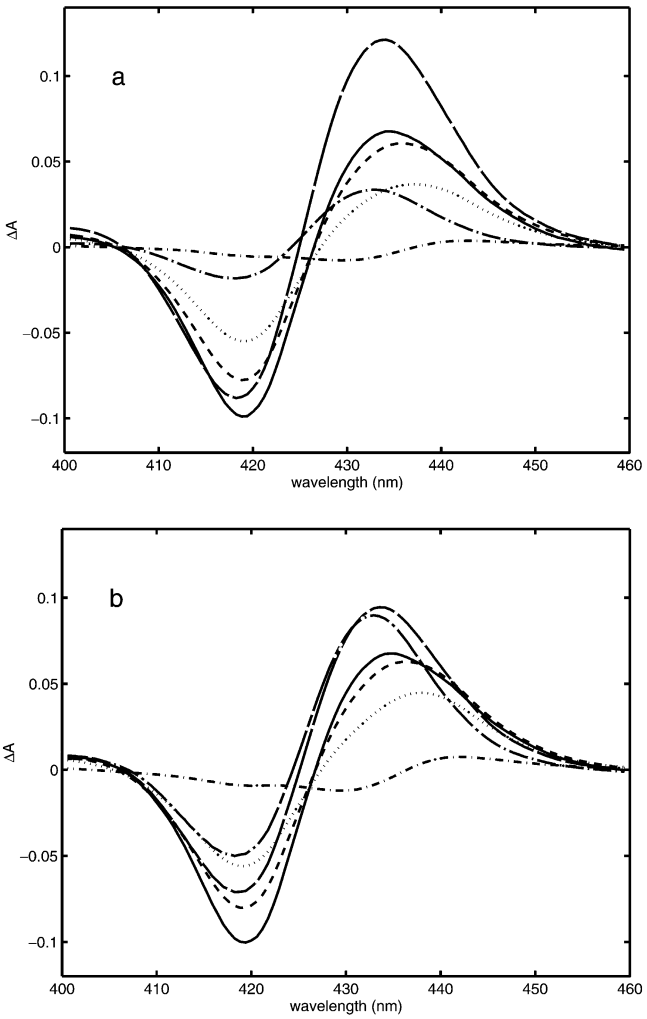

FIGURE 7: Model-independent decay spectra calculated from a 6-exponential fit to photolysis data for HbCO (a) strippped and (b) + IHP. Spectra for decay τ's: τ_1 (−), τ_2 (- - -), τ_3 (- · -), τ_4 (···), τ_5 (— —), τ_6 (- — -) (numbering as in Table 3).

Table 3: Effect of IHP on Observed Time Constants and Spectral Amplitudes from Simple 6-Exponential-Decay Global Fitting of HbCO Soret Band Photolysis Data[a]

	τ_1	τ_2	τ_3	τ_4	τ_5	τ_6
HbCO[b]	0.025	0.10	1.5	40	130	2800
	(0.24)	(0.20)	(0.02)	(0.17)	(0.32)	(0.08)
HbCO[b] + IHP[c]	0.027	0.12	2.4	41	200	5200
	(0.22)	(0.19)	(0.03)	(0.14)	(0.22)	(0.19)

[a] Time constants are in μs, fractional amplitudes (proportional to the vector norms of the decay spectra) are listed in parentheses. [b] Conditions: 120 μM heme, pH 7.4, 0.1 M Tris, 0.1 M NaCl, 1 mM EDTA, 20 °C. [c] 2 mM IHP.

tion to the R and T states were both lengthened (50% and 90%, respectively) by the addition of IHP (Table 3). Such observations have posed a challenge for the MWC model (*32*, *33*). An allosteric effector such as IHP would not be expected to directly influence the binding rates and affinities of the R and T states in the simplest two-state models, which posit that only the rates and equilibria for interconversion of the quaternary states are directly modified by effectors. A natural mechanism for a direct role for allosteric effectors in controlling the T-state recombination kinetics is provided by the MLFER model, as discussed below.

The optimized values of the MLFER parameters obtained from a simultaneous fit to kinetic data for stripped and IHP-bound HbCO are presented in Table 2. The optimized values were close in each case to the respective trial values expected from the a priori considerations given above. A statistical analysis testing the stability of the fits was carried out by addition of normally distributed noise (standard deviation = 0.3 kcal) to the experimental $^{ij}\Delta G_c$ and ΔG_{IHP} energy values that were used as fixed inputs to the model. (The signal-to-noise ratio of the spectrokinetic data, being greater than 100, was much larger than the corresponding ratio of the thermodynamic data, ~20. Hence, the energy uncertainties were deemed the dominant source of instability in the modeling.) The statistically averaged values of the allosteric parameters were identical to the values optimized for the energy values given above within the uncertainties of the α ($\pm$10%) and rate constant ($\pm$20−30%) parameters, allowing us to conclude that the results of the MLFER kinetic model were stable with respect to experimental noise.

The essential spectrokinetic features of HbCO's post-photolysis recombination and relaxation processes were accurately captured by the model, as can be seen by the very close fits to the global time evolutions for both allosteric effector conditions, stripped vs IHP (see panels d−f in Figures 5 and 6). The modeling of the geminate and bimolecular recombination reactions was most clearly demonstrated by the excellent fits to the first **V** vector for each case, whereas the success of the model in reproducing the second and third vectors demonstrated good accuracy in modeling the structural relaxation kinetics.

The central result of the MLFER model is the deconvolution of microstate allosteric transition rates (Table 4). The calculated $^{ij}k_{RT}$ values decreased with increasing ligation and increased in the presence of IHP, as expected. However, the variation of rate constant with ligation number was well described by the simple two-state expression $k_{RT}(i) = k_{RT}(0)/d^i$, where i is the number of ligands bound, only for ligation states with $i \neq 2$ (Figure 8). Deviating from simple two-state behavior, the R→T rates of the $i = 2$ microstates bifurcated such that the $^{21}R \rightarrow {}^{21}T$ rate constant was similar to the $^{\{11,12\}}R \rightarrow {}^{\{11,12\}}T$ rate constant, and the $^{\{22,23,24\}}R \rightarrow {}^{\{22,23,24\}}T$ rate constant was closer to the $^{\{31,32\}}R \rightarrow {}^{\{31,32\}}T$ value, whereas their geometric mean lay close to the two-state line. This bifurcation of the calculated rates for $i = 2$ is a direct consequence in the MLFER model of the split in the thermodynamic energies of the doubly ligated T microstates. The T→R rate constants depended much more strongly on ligation number than did the R→T rate constants, increasing by 10^7 over the range $i = 0$ to 4, albeit their values also had larger margins of uncertainty (see Table 4). They were also affected more dramatically by the presence of IHP, decreasing by a factor of 10^{-3} for $i = 0$.

The CO recombination rate constants calculated from the MLFER model for the T microstates were very heterogeneous, ranging from a low value of 0.2 μM^{-1} s^{-1}, for the reaction $^{21}T + CO \rightarrow {}^{\{31,32\}}T$, to a high value of 5 μM^{-1} s^{-1}, for $^{\{11,12\}}T + CO \rightarrow {}^{21}T$ (Table 5). In other words, the recombination of CO with a T_1 microstate to form the ^{21}T microstate proceeded ~25 times faster than the next step in the recombination chain, the reaction of CO with ^{21}T to form a T_3 microstate. Indeed, the former rate constant was only a factor of 2 smaller than that of the R states. The T-microstate

Table 4: Microstate R→T and T→R Quaternary Transition Rate Constants Calculated from MLFER Model[a]

	$^{ij}k_{RT}$		$^{ij}k_{TR}$	
[*ij*]	stripped	IHP	stripped	IHP
[01]	$1.6 \pm 0.4 \times 10^4$	$1.0 \pm 0.2 \times 10^5$	0.3 ± 0.2	$3.5 \pm 2.5 \times 10^{-4}$
[11],[12]	$5 \pm 1 \times 10^3$	$1.9 \pm 0.4 \times 10^4$	24 ± 18	0.16 ± 0.15
[21]	$4 \pm 1 \times 10^3$	$9 \pm 2 \times 10^3$	75 ± 45	2.6 ± 1.7
[22],[23],[24]	$1.1 \pm 0.4 \times 10^3$	$2.6 \pm 0.8 \times 10^3$	$8 \pm 6 \times 10^3$	$3 \pm 2 \times 10^2$
[31],[32]	$6 \pm 3 \times 10^2$	$9 \pm 5 \times 10^2$	$9 \pm 4 \times 10^4$	$1.6 \pm 0.8 \times 10^4$
[41]	$3 \pm 2 \times 10^2$	$4 \pm 2 \times 10^2$	$1.2 \pm 0.8 \times 10^6$	$9 \pm 6 \times 10^5$

[a] Rate constants are in s^{-1}.

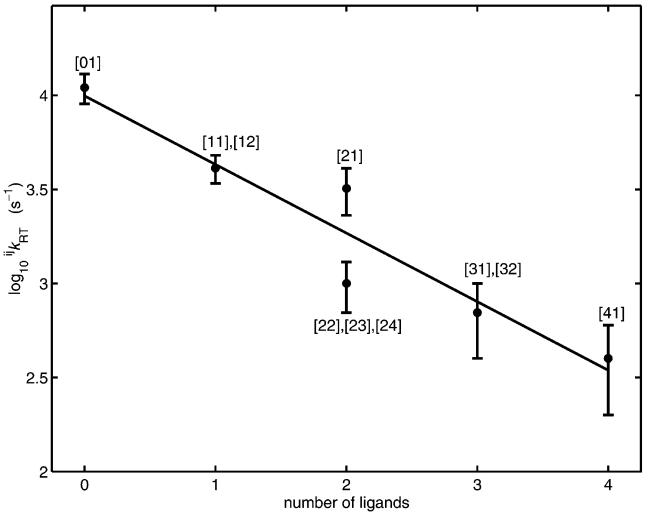

FIGURE 8: Semilog plot of microstate R→T rate constants calculated from MLFER model vs number of CO ligands.

Table 5: Microstate Bimolecular CO Recombination Rate Constants Calculated from MLFER Model[a]

	stripped	IHP
k_R	10 ± 3	10 ± 3
$^{01\rightarrow11}k_T$	0.8 ± 0.3	0.3 ± 0.1
$^{11\rightarrow21}k_T$	5 ± 2	1.9 ± 0.6
$^{11\rightarrow22}k_T$	0.4 ± 0.1	0.15 ± 0.05
$^{21\rightarrow31}k_T$	0.18 ± 0.02	0.067 ± 0.006
$^{22\rightarrow31}k_T$	2 ± 1	0.9 ± 0.2
$^{31\rightarrow41}k_T$	3 ± 1	1.4 ± 0.6

[a] Rate constants are in μM^{-1} s^{-1}.

bimolecular rate constants calculated for stripped HbCO are graphed logarithmically in Figure 9, wherein the widely distributed rate constants calculated for the individual microstates clustered roughly around the nominal T-state value (T) calculated from τ_6 of the phenomenological 6-exponential fit.

Note that the rates inferred here imply a cooperativity in ligand binding that is independent of the classical two-state mechanism. Binding of the first ligand to T_0, for instance, enhanced the rate of binding of a second ligand (to form the ^{21}T microstate) by a factor of 6. The latter binding event was in turn anticooperative, as the binding rate constant then decreased by the factor of 25 mentioned above. This change in ligand binding rate concomitant with T-state ligation is not much smaller in magnitude than the change traditionally associated with transformations between the R and T quaternary states. Similarly, the rates reported here also indicate that IHP binding had a direct effect on the T-state CO-binding rate constants, decreasing them by a factor of 2−3. A similar direct effect on the CO-binding bimolecular

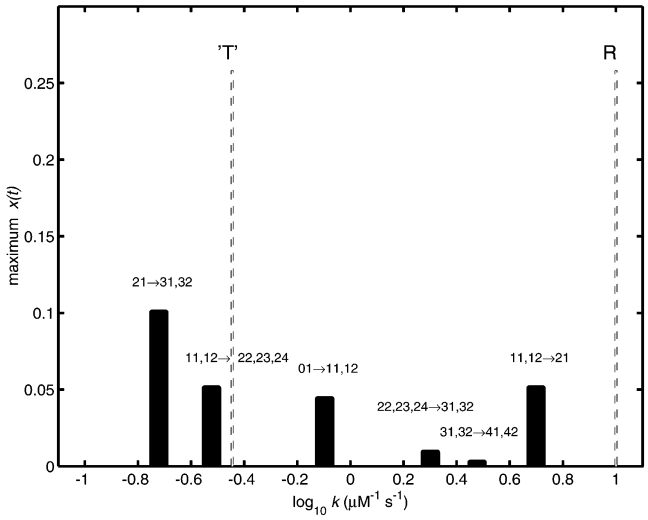

FIGURE 9: Semilog histogram of microstate bimolecular CO-binding rate constants. The solid bars show the distribution of T-microstate rate constants, where maximum $x(t)$ is the maximum fractional concentration of the reacting microstate. The dashed bar labeled 'T' indicates the traditional T-state rate constant from a phenomenological 6-exponential fit, its height reflecting the total T-microstate fractional concentrations. The R-microstate rate constant is included for comparison (dashed bar labeled R).

rate constant of T-state deoxy HbA was measured previously for IHP in a stopped-flow mixing study (*34*).

The concentrations calculated for the R states evolved with time largely as expected for sequential ligand binding, the concentration peaks appearing in the temporal order R_0, R_1, R_2, R_3 ($R_2 = {}^{21}R + {}^{2j}R$) before R_3 recombined to form the starting material, R_4 (Figure 10). The higher peak concentration of R_1 compared with that of R_0 mainly reflected the higher statistical probability of producing a singly liganded tetramer after geminately recombining 30% of the heme sites, although the higher statistical factor for bimolecular CO recombination and the higher rate constant for R→T transformation also contributed to speeding the R_0 rate of decay and limiting its peak concentration. The addition of IHP accelerated the rate of decay and decreased the magnitudes of the peak concentrations for all of the R microstates (see Figure 10b).

The calculated T-state evolution, on the other hand, was more complicated principally because the ^{21}T microstate acted as a kinetic bottleneck. This role would be consistent with its enhanced rate of production compared with the other T microstates, both by R→T conversion and CO recombination, and its decreased rate of decay through CO recombination noted above. The ^{21}T microstate thus dominated the T-state concentration dynamics under both of the effector conditions investigated (Figure 11). Indeed, the role of this

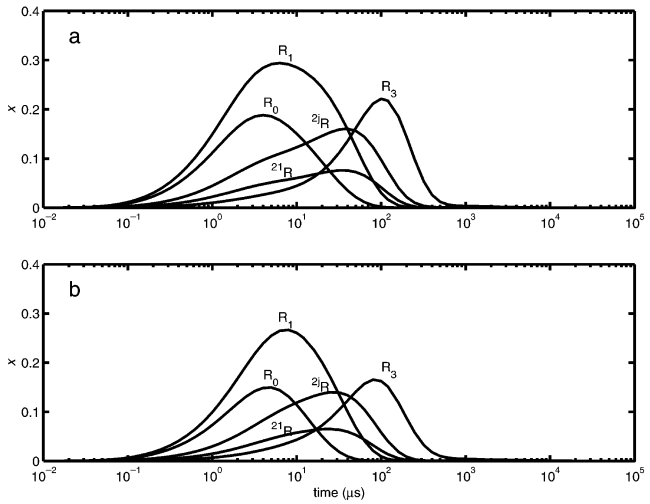

FIGURE 10: Calculated concentrations of R microstates vs time for HbCO (a) strippped and (b) + IHP.

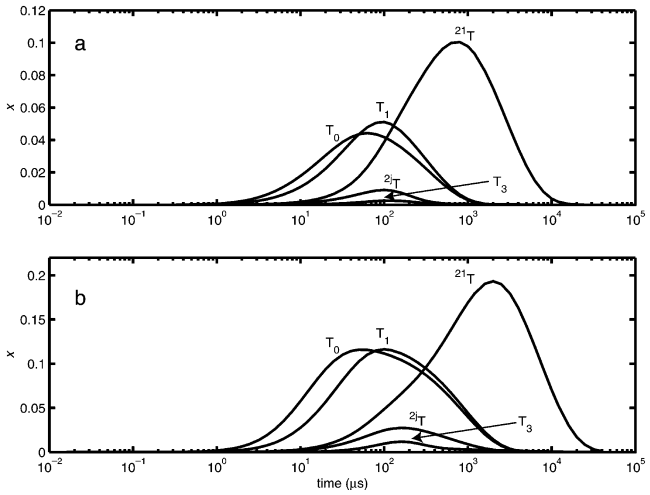

FIGURE 11: Calculated concentrations of T microstates vs time for HbCO (a) strippped and (b) + IHP.

microstate in the recombination kinetics appeared to be so dominant that the calculated concentration profiles for the remaining T_2 microstates (^{2j}T) and the subsequently formed T_3 states were nearly negligible. The addition of IHP did not qualitatively change this scenario, although overall T-state production doubled, consistent with the faster R-state decay mentioned above. The longer time required for T-state decay simply reflected the decrease in CO recombination rate constants reported above for IHP.

The MLFER model calculated concentration dynamics for the R_r, R_t, R, and T heme conformational types (Figure 12) reflecting the overall effect of IHP on the R and T state kinetics inferred above: the photolyzed R-type hemes decayed more rapidly in the presence of IHP to produce about twice as many T-type hemes, which in turn decayed through CO recombination more slowly. The calculated spectra of the four heme types show the expected progression in the position of the deoxy peak wavelength to increasingly shorter wavelength as the protein structure near the heme pocket relaxed after ligand photodissociation (Figure 13a). The band shape of the calculated T−R difference spectrum was very similar to that of the equilibrium T−R difference spectrum over the 430−450 nm spectral region (Figure 13b). This was an expected consequence of the spectral fitting penalty,

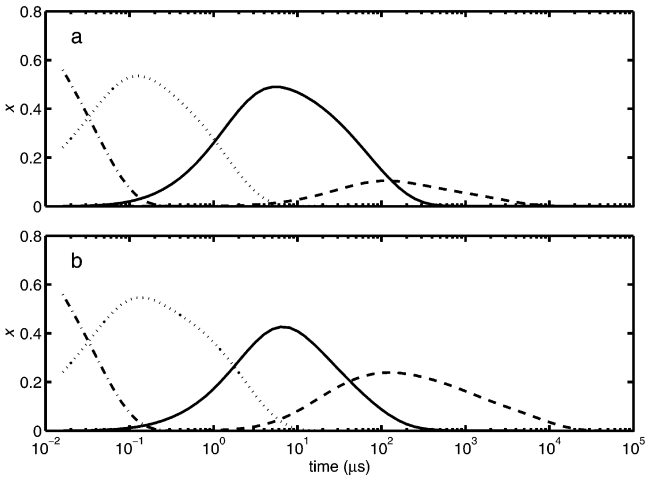

FIGURE 12: Calculated concentrations of heme conformational species R_r (-•-), R_t (••••), R (−), and T (- -) vs time for HbCO (a) strippped and (b) + IHP.

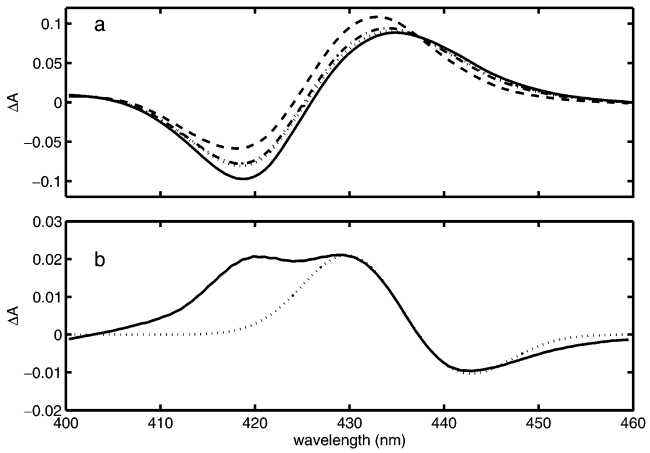

FIGURE 13: (a) Calculated spectra of heme conformational species for HbCO (average of stripped and IHP) labeled as in Figure 12 legend. (b) Calculated T−R difference spectrum (−) and equilibrium T−R difference spectrum (••••) from Perutz et al. (*50*). The latter spectrum is scaled to the vector norm of the calculated spectrum over the 435−450 nm spectral region, as in the calculation of the spectral fitting penalty, ρ, described in the text.

derived from a comparison of these two spectral shapes, that was used in the kinetic modeling procedures to constrain the T and R spectra. (The second peak appearing at the carboxyheme peak wavelength, 419 nm, in the calculated spectrum is attributed to a stray light artifact associated with the spectrograph (*17*).)

DISCUSSION

The overall program of the MLFER kinetic model is the systematic application of linear free energy relations (LFERs) to the kinetics of ligand binding and quaternary structure change on the ligation microstate level in hemoglobin. The first application of LFERs to hemoglobin's ligand binding reactions was due to Szabo (*35*). He proposed that α values of about 0.1, 0.4, and 1 described the variation of the binding "on" rate constant for the ligands O_2, CO, and NO, respectively, as a function of variations in the binding equilibrium constants as the protein structure changes between the R and T quaternary states. Similar values were found for the variations of O_2 and CO binding rate constants to tetraphenylporphyrin heme models in toluene as a function

of "basket handle" and "picket fence" structural perturbations to the binding equilibrium constants (*36*). The LFER approach was applied to the R→T transition rate constant by Eaton et al. (*6*), who found that an α value of 0.17 ± 0.02 described its variation in response to allosteric effectors and ligand binding. Later HbCO photolysis studies have also reported similar values (*7*, *37*, *38*).

With the concepts established that the variation of ligand binding rate constants with quaternary structural change and the variation of structural transition rate constants with ligand binding can both be described in hemoglobin by LFERs, the combination of these reciprocal perturbative relationships into a systematic microscopic description of hemoglobin's allosteric dynamics then only requires microscopic knowledge of the corresponding thermodynamic quantities, the free energies of ligand binding and structural change. This knowledge became available in large part for the case of HbCO with the microstate thermodynamic measurements of Huang and Ackers (*9*). When the cooperative free energies of the 10 equilibrium ligation microstates were measured, those results gave access, via thermodynamic linkage to the ligand affinity of the free dimers, many of the requisite ligation microstate binding energies. However, determining the remaining binding energies and all of the quaternary structural transition energies requires additionally knowing the ${}^{ij}\Delta G_c$ values of the remaining 10 metastable ligation microstates representing the higher energy quaternary conformer of each stable ligation microstate. Those values were estimated in the MLFER model from additional experimental information, whenever available, or from interpolations and extrapolations of the experimental values, as described above.

The most fundamental test of the MLFER approach afforded by the experimental results presented here is a comparison of the α_{RT} and α_{CO} values determined from the model to the values determined previously by the more macroscopic (microstate averaged) studies cited above. Although some differences could be expected between α parameters determined from macroscopic and microscopic kinetic models, too large a difference would suggest that the microscopic energies used here were unrealistic and that the α_{RT} and α_{CO} parameters served merely as arbitrary fitting parameters. The α_{RT} value found here, 0.21 ± 0.03, is about 20% larger than values previously reported (e.g., 0.17 ± 0.02) (*6*). However, this small difference can probably be attributed to the neglect of dissociated dimers in previous studies, as it vanishes when tetramer dissociation to dimers is also neglected in the MLFER model (results not shown). Thus, the correspondence found here between previous macroscopic and the current MLFER values for both α_{RT} and α_{CO} is close and suggests that the microstate energy values used are indeed reasonably realistic, although some cancellation of errors among neglected factors may contribute to this agreement, as discussed further below.

The central assumption made in arriving at the free energy values used in the model was the extrapolation of the ${}^{ij}\Delta G_c$ value of the stable (in stripped HbCO) R microstates, ${}^{\{22,23,24\}}$R and ${}^{\{31,32\}}$R, (6.5 kcal/mol) to the metastable R states, ^{01}R, ${}^{\{11,12\}}$R, and ^{21}R. The approximation that the R microstates have essentially identical cooperative free energies, in contrast to the large differences between the T microstate energies, is consistent with the much weaker dimer−dimer interactions present in the R microstates. Free dimers are noncooperative; therefore, it is the strong constraints imposed by the T-state interactions that provide the resistive force underpinning the large changes in conformational energy caused by ligand binding. (Note that this picture implicitly takes the view of Shulman and others (*39*) that T-state conformational strain energies are delocalized to a large extent throughout the tetramer, as opposed to being strictly localized to the progressive breaking of dimer−dimer interactions with ligation first proposed by Perutz (*40*). The delocalization of strain (which the intra-dimer cooperativity inferred in the present work suggests remains localized mainly to the ligated dimer) implies that the T dimer−dimer contacts tend to resist deforming forces more stiffly than other conformational degrees of freedom in the protein and are thus less able to store strain energy.) The dimer−dimer contacts are energetically weaker (e.g., by 6.5 kcal/mol for ^{01}R relative to ^{01}T) and apparently much less conformationally constrained in the R than in the T state; however, they are still finite (∼8 kcal/mol) (*9*). Thus, we cannot rule out the possible presence of significant (>0.3 kcal/mol) cooperative free energy differences between the stable and metastable R microstates. In particular, the small quaternary enhancement evident in ${}^{41}\Delta G_c$(R) relative to the R_3 free energies (0.3 kcal/mol stabilization) may be echoed in small enhancements of R_2 vs R_1 or R_1 vs R_0. Also in this regard, some reported L_0 values suggest that ${}^{01}\Delta G_c$(R) is a little larger than 6.5 kcal/mol in the presence of 0.1 M Cl^- (*24*). (Note that any direct effect of IHP on R-state cooperative free energies and ligand binding kinetics has also been neglected in the model for simplicity, although there is evidence that such effects may be significant (*30*, *32*).)

The roles of chloride ion and IHP as allosteric effectors are straightforward, as described above in the model, but become more ambiguous when one considers that the present experiments started with HbCO in the R conformation before photodissociation. Even if effector binding is diffusion controlled, there probably is not enough time after photodissociation and the subsequent conversion of R conformers to T for the reequilibration of effector binding. Thus, the kinetic behavior of the T microstates reported here probably reflects R-state levels of effector binding, whereas the thermodynamic energies used in the model pertain to effector-equilibrated states. Nonetheless, given the high concentrations of chloride ion and IHP used relative to the respective R-state effector binding affinities (*26*), we expect that effector binding was reasonably close to stoichiometric (95% for IHP binding). (The R_4 binding affinity of Cl^- does not seem to be available. Hence, by analogy with IHP and DPG, we assumed that the R_4 binding affinity was approximately equal to the square root of the known T_0 affinity.)

Having established the overall validity of the MLFER approach to kinetic modeling in HbCO, we now examine more detailed features of the model. In particular, we are interested in the kinetic consequences of the splitting of the T_2 microstate energies, the free energy of placing both ligands on the same dimer (^{21}T) being several kcal lower than placing a ligand on each dimer. The latter thermodynamic observation is at the core of the symmetry model for hemoglobin allostery of Ackers and co-workers. Can we distinguish kinetic correlates as well? To answer this question, we made two comparisons. First, we compared the MLFER model to

Table 6: Comparison of Fit Qualities for Microstate and Two-State LFER Kinetic Models[a]

model	$f + \rho$
MLFER	0.025 ± 0.004
TLFER	0.053 ± 0.007
modified TLFER	0.036 ± 0.008

[a] Fit quality was measured by the quantity $f + \rho$. f, the sum of the residuals squared, is defined in eq A15. The T−R spectral fitting penalty $\rho = 0.1 \cdot \sum (\mathbf{H}_{i4} - \mathbf{H}_{i3} - \mathrm{D}_i)^2$, where $\mathbf{H}$ is the matrix of heme spectra in eq A16 and $\mathbf{D}$ is the equilibrium T−R difference spectrum normalized to the vector norm of $\mathbf{H}_4 - \mathbf{H}_3$ (calculated T−R difference spectrum after photolysis).

the simplest two-state model that still retained LFERs for ligand binding and allostery. In this two-state LFER (TLFER) model, the T microstate energies used above were replaced by free energies that increased with ligation in equal increments between the same endpoints as those used in the MLFER model (i.e., $\Delta G_c^{\mathrm{two-state}}(\mathrm{T}_i) = (i/4)11$ kcal/mol). (Note that all the models compared here used the same number of free parameters.) This is a classical two-state model in the sense that the equal spacing of the T levels removes any cooperativity in ligand binding that is independent of the R to T transition. In particular, setting the T_2 microstate energies equal to one another implies loss of the large intradimer cooperativity underlying the symmetry rule for quaternary structural switching. A second, closer comparison was also made to a modified TLFER model in which all of the MLFER ${}^{ij}\Delta G_c$ values were retained except for ${}^{21}\Delta G_c(\mathrm{T})$, which was set equal to the value used for the remaining T_2 microstates (7.9 kcal in stripped HbCO). (Although other values for equal T_2 microstate energies could be used, this value was determined to be the least disruptive to the quality of the kinetic fits.) The modified TLFER model thus retained some of the sequential T-state cooperativity inherent in the MLFER model, but discarded the T_2 energy gap, the major manifestation of intradimer cooperativity. As can been seen from the results in Table 6, both "two-state" models produced significantly poorer fits to the data than did the MLFER model. The modified model performed significantly better than the simplest TLFER model, however, implying that the inclusion of both novel features of the MLFER model, T-state cooperativity in general and its large intradimer component (the symmetry rule) in particular, is important in arriving at the most accurate description of HbCO kinetics.

A surprising kinetic consequence of the T-state cooperativity inherent in the MLFER model is the prediction that ligand recombination to the singly liganded T quaternary structure proceeds nearly as rapidly as R-state rebinding. Although we are aware of no precedent for this kinetic assignment in hemoglobin, the identification of a fast component in the distribution of T-microstate rebinding rate constants may provide an explanation for a longstanding puzzle in HbCO ligand binding kinetics: the appearance of heterogeneous rebinding rates for the R state. This heterogeneity is exemplified by the observation of two rebinding time constants in the 100−300 μs time regime in 7- and 8-exponential phenomenological fits of HbCO photolysis kinetics (*41*). A second piece of this puzzle is the sensitivity of this apparent R-state heterogeneity to the presence of allosteric effectors (*42*). This kinetic heterogeneity has traditionally been attributed to different α and β chain affinities within the tetramer, which are expected to correlate with different binding rate constants. The β chains typically, but not always, have been assigned the higher affinity, as observed directly for the isolated chains (*29*). Yet, significant chain differences are not observed in any of the post-photolysis kinetic phases of cobalt−iron hybrid HbCO tetramers (*43*) nor in the geminate rebinding dynamics of native HbCO (*44*). The results of two-state kinetic modeling of HbCO photolysis carefully elaborated to distinguish α,β chain differences also indicate that there is very little difference in their rebinding kinetics (*7*). In this light, the present results suggest that the fast "β-chain" rebinding phase ($\tau \sim 100$ μs) is actually due to R-state rebinding to both types of chains, whereas the slow "α-chain" rebinding phase ($\tau \sim 300$ μs) is due to the atypically rapid T-state rebinding reaction $\mathrm{T}_1 + \mathrm{CO} \rightarrow {}^{21}\mathrm{T}$. This reassignment would also naturally explain the other heretofore puzzling aspect of the putative R-state kinetic heterogeneity, the ability of IHP and other effectors to slow the α-CO binding rate constant but not the β-CO rate constant (*28*).

The sensitivity of the kinetic modeling results to the effects of T-state cooperativity points out the inherent advantage of kinetic techniques over equilibrium ligand binding measurements such as saturation measurements in evaluating models of cooperativity. Historically, the most compelling evidence for the two-state model has come from the kinetic experiments of Sawicki and Gibson (*8*), which identified only two species after photolysis, a slow (T) and a fast (R) ligand-rebinding form, regardless of the distribution of ligation states created. In contrast, the MWC and KNF models of hemoglobin cooperativity have been more difficult to distinguish by use of equilibrium measurements. Similarly, significant T-state cooperativity has not been observed in equilibrium measurements of oxygen binding to T-state crystals, which found that the Hill parameter $n = 1$ (*45*, *46*). However, the T-state cooperativity predicted by the MLFER model is a "zero-sum game" in that the cooperative enhancement of the rate constant for the reaction $\mathrm{T}_1 + \mathrm{CO} \rightarrow {}^{21}\mathrm{T}$ is immediately offset by the roughly equal disenhancement of the rate constant for the subsequent reaction ${}^{21}\mathrm{T} + \mathrm{CO} \rightarrow \mathrm{T}_3$. Hence, these effects are expected to largely cancel from aggregate equilibrium measures of cooperativity such as the Hill n value. The greater sensitivity of kinetic measurements in this regard arises from the ability to study appreciable populations of ligation intermediates that can be distinguished from one another by differences in their dynamics, as opposed to studying aggregate equilibrium populations that are dominated by the reaction end states.

While advancing the propositions of T-state cooperativity and the symmetry rule contained in the MLFER model, we are also retaining the most basic feature of the two-state model, the equilibrium between two quaternary structures. In the MLFER model, the binding of ligands shifts the equilibrium between the R and T conformers through T-conformer strain forces that are primarily localized within each dimer. A possible mechanistic scenario rationalizing this localization is based on the premise that the $\alpha_1\beta_2$ interactions are strong enough in the T conformation to resist changes in interdimer structure upon binding of the first ligand as forces pushing for such changes are transmitted from the heme pocket to the interface by motion of the

Scheme 3

Heme Type	$[Fe\cdots CO]_r$	$[Fe\cdots]_r$	$[Fe\cdots CO]_t$	$R_{t,0}$	R_0	T_0	$R_{t,1}$	R_1	T_1	$R_{t,2}$	Intermediate ^{21}R	Intermediate $^{\{22,23,24\}}R$	Intermediate ^{21}T	Intermediate $^{\{22,23,24\}}T$	$R_{t,3}$	R_3	T_3
R_r	4	4	0	0	0	0	0	0	0	0	0	0	0	0	0	0	0
R_t	0	0	4	4	0	0	3	0	0	2	0	0	0	0	1	0	0
R	0	0	0	0	4	0	0	3	0	0	2	2	0	0	0	1	0
T	0	0	0	0	0	4	0	0	3	0	0	0	2	2	0	0	1

F-helix. The resulting strain is accommodated in this scenario by distortion of the ligated subunit's tertiary structure as its heme pocket is allowed to move toward the $\alpha_1\beta_2$ interface while the T-state dimer-dimer contacts are preserved. Because the subunits within a dimer are bound together very tightly at the $\alpha_1\beta_1$ interface, much of the tertiary distortion induced in the first subunit could plausibly be echoed by roughly parallel distortions in the second subunit as it is tugged by the first at their common interface. A second ligand can then bind to a subunit in this dimer more easily than to subunits in the unligated dimer, the former being already partially accommodated to the ligated tertiary structure, whereas binding to the latter would require perturbing both remaining subunits. If the second ligand does bind to the unligated dimer, the free energy stored within each strained dimer will exceed the free energy difference between the R and T conformations of the $\alpha_1\beta_2$ interface (at least in stripped hemoglobin), triggering the T→R transition (the symmetry rule).

The major cooperativity effects in ligand binding are still mediated by the two-state equilibrium in the symmetry rule model (and its kinetic analogue, the MLFER model), but cooperativity within the quaternary states, particularly the T conformer, cannot be neglected either. The important advantage gained in admitting this complication to the two-state model, besides a more realistic description of hemoglobin allostery, is the simplification afforded by using the microstate cooperative energies as a guide to the kinetics. In the present case, the complete post-photolysis kinetics of HbCO in two very different effector conditions can be well described by a MLFER model that uses only 8 free parameters and less than 20 intermediates. Moreover, the values of at least 4 of these parameters, α_{RT}, k_{RT}, α_{CO}, and k_R are expected to apply to a wide variety of effector conditions. It will be interesting to test this prediction of the MLFER model against kinetic data for a wider variety of perturbations such as pH, inorganic anions, and organic phosphates, in addition to IHP.

In summary, we have applied a novel model combining the LFER paradigm (*5*, *6*, *35*) and advances in the thermodynamic characterization of hemoglobin cooperativity (*1*) to describe the photodissociation kinetics of HbCO on the microstate level. The excellent fit to the kinetic data and the agreement of the rate constants obtained here with those found in previous studies support the validity of this approach. However, even stronger support is found in the remarkably close correspondence of the α values determined from the fitting with those found in previous studies. These correspondences imply strongly that the thermodynamic energies reported by Huang and Ackers directly underlie the allosteric dynamics observed here. Accordingly, the model confirms specific kinetic features predicted by those energies such as cooperative ligand binding within the T microstates and the importance of the ^{21}T microstate as a bottleneck during ligand rebinding reactions. It also provides a natural mechanism for incorporating the direct effect of allosteric effectors on the ligand affinity and binding rate of the T quaternary structure. This feature of hemoglobin allostery implies direct communication between the (homotropic) heme and heterotropic effector binding sites via conformational plasticity within the T quaternary state (*47*); hence, it has been difficult to explain with simple two-state models (*48*).

The utility of the model presented here is 2-fold: (1) it promises to systematize the study of hemoglobin dynamics via a small number of MLFER relation parameters that are universal for a large class of perturbations, and (2) it provides the ability to test microscopic details of allosteric dynamics. Most interesting in the latter regard is the question of the symmetry rule for quaternary change that has been deduced by Ackers and co-workers from the thermodynamic evidence. We find that fitting with a kinetic model that does not include the energy splitting between T_2 microstates that is implied by the symmetry rule gives a significantly poorer fit to the data than one that does include the symmetry rule. Statistically significant as this independent support for the symmetry rule is, however, we recognize that it may not be dramatic enough to decisively settle such an important question. Therefore, more compelling evidence, obtained from application of the model to kinetic data from iron−cobalt hemoglobin hybrids, is presented in a companion paper (*10*).

APPENDIX

Coupling of Schemes 1 and 2. Scheme 1 (per heme basis) and Scheme 2 (per tetramer basis) were coupled by use of combinatorial statistics to describe the distribution of photolyzed hemes remaining within a tetramer after geminate recombination. The relative populations of the $R_{t,n}$ species produced by geminate recombination are a simple function of p (net photolysis yield) and n given by

$$P_n = \frac{4!}{(4-n)!n!}\, p^{4-n}(1-p)^n \qquad \text{(A1)}$$

The connections between Scheme 1 and Scheme 2 are then made explicit by replacing the reaction step

$$[\mathrm{Fe}\cdots\mathrm{CO}]_t \xrightarrow{k_6} [\mathrm{Fe}\cdots]_t$$

with the four steps

$$[\mathrm{Fe}\cdots\mathrm{CO}]_t \xrightarrow{C_0 k_6} \mathrm{R}_{t,0} \tag{A2}$$

$$[\mathrm{Fe}\cdots\mathrm{CO}]_t \xrightarrow{C_1 k_6} \mathrm{R}_{t,1} \tag{A3}$$

$$[\mathrm{Fe}\cdots\mathrm{CO}]_t \xrightarrow{C_2 k_6} \mathrm{R}_{t,2} \tag{A4}$$

$$[\mathrm{Fe}\cdots\mathrm{CO}]_t \xrightarrow{C_3 k_6} \mathrm{R}_{t,3} \tag{A5}$$

where the statistical factors C_n are given by

$$C_n = nP_n / \sum_{n'=0}^{3} n'P_{n'} \tag{A6}$$

and by making a similar replacement for

$$[\mathrm{Fe}\cdots]_r \xrightarrow{k_3} [\mathrm{Fe}\cdots]_t:$$

$$[\mathrm{Fe}\cdots]_r \xrightarrow{C_0 k_3} \mathrm{R}_{t,0} \tag{A7}$$

$$[\mathrm{Fe}\cdots]_r \xrightarrow{C_1 k_3} \mathrm{R}_{t,1} \tag{A8}$$

$$[\mathrm{Fe}\cdots]_r \xrightarrow{C_2 k_3} \mathrm{R}_{t,2} \tag{A9}$$

$$[\mathrm{Fe}\cdots]_r \xrightarrow{C_3 k_3} \mathrm{R}_{t,3} \tag{A10}$$

Optimization of Model Parameters in Fitting of Kinetic Data. The full kinetic model comprising the geminate and allosteric reactions (Schemes 1 and 2 combined via eqs A1−10) can be represented by a matrix of rate constants **K** in the symbolic first-order rate equation

$$\frac{\mathrm{d}\mathbf{c}(t)}{\mathrm{d}t} = \mathbf{K}\boldsymbol{c}(t) \tag{A11}$$

where $\boldsymbol{c}(t)$ is a column vector containing the time-dependent concentrations of the species in the combined Schemes 1 and 2. Matrix techniques were then used to solve eq A11 for the concentrations given the starting condition $c_1(0) = c_0$ (*49*), where $c_1(0)$ was the initial concentration of the prompt geminate species $[\mathrm{Fe}\cdots\mathrm{CO}]_r$ and c_0 was the total HbCO concentration (assuming complete photodissociation before geminate recombination.)

Our goal was to find the parameter values in **K** that produce the best fit to the data matrix **A** (indexed by wavelength and time) in

$$\mathbf{A} = \mathbf{BC} \tag{A12}$$

where the columns of **C** are the values of $\boldsymbol{c}$(t) evaluated at the experimental delay times and the columns of **B** are the spectra of the kinetic intermediates. In principle, the optimization could be carried out directly using eq A12, but it was more efficient to first decompose **A** into separate spectral and temporal matrixes and use the latter more compact representation of the kinetic data.

Starting with chemically reasonable values for the model parameters, the parameters were varied in a search (simplex algorithm) for the set of values that optimized the fit of the concentration kinetics to the time course of the data (i.e., minimizing the sum of squares of the deviations (*f*) between the time course and the calculated fit). This optimization was global over time and wavelength in that the time course was represented by a matrix **V** obtained from singular value decomposition (SVD) of the data matrix **A**, the former matrix being indexed by time and SVD component number (*11*). In the SVD expression

$$\mathbf{A} = \mathbf{USV}' \tag{A13}$$

S is a diagonal matrix of nonnegative singular values (spectrokinetic magnitudes of the orthogonal SVD components), **U** contains the orthonormal SVD spectral basis functions as columns, and **V**′ is the transpose of the matrix of orthonormal temporal basis functions, **V**. The SVD components were truncated to the *r*th largest singular values to obtain the approximate decomposition of the data matrix

$$\mathbf{A}_r = \mathbf{U}_r \mathbf{S}_r \mathbf{V}_r' \tag{A14}$$

The function to be minimized is then

$$f = \sum_{ts} \mathrm{S_{ss}}^2 (\mathrm{V_{ts}} - [(\mathbf{MC})' \cdot \mathrm{pinv}(\mathbf{MC})' \cdot \mathbf{V}_r]_{ts})^2 \tag{A15}$$

where *t* and *s* index a double sum over delay times and SVD component number, respectively, and the sum over *s* is truncated at $s = r$. The indexed matrix element expression in square brackets represents the best least-squares fit to the observed temporal data in $\mathbf{V}_r$, using the heme chromophore-type time-evolution functions in **MC**, where pinv(**MC**) is the Moore-Penrose pseudoinverse of **MC**. **M** is a matrix (Scheme 3) indexed by heme spectral type and kinetic species number. Its effect in eq A15 is to constrain the fit to use only four possible photolysis difference spectra for the photolyzed hemes, labeled R_r, R_t, R, and T. The latter correspond to the four conformationally distinct heme sites recognized in the model: the prompt photolysis product, the product of geminate tertiary relaxation, the product of early $\alpha_1\beta_2$ interfacial relaxation, and the product of full quaternary relaxation, respectively. Thus M_{ij} corresponds to the number of heme sites of spectral type *i* contained in a tetramer corresponding to the kinetic species *j*. This procedure improved the stability of the fits by greatly reducing the number of intermediate spectra calculated by the model relative to the maximum possible, the latter being equal to the total number of photodissociated species in Schemes 1 and 2 ($n = 17$). The heme component spectra (columns of **H**) were calculated from

$$\mathbf{H} = \mathbf{A}_r \,\mathrm{pinv}(\mathbf{MC}) \tag{A16}$$

The spectra of the individual intermediates in Equation A12 are obtained from

$$\mathbf{B} = \mathbf{HM} \tag{A17}$$

Finally, an additional constraint was added to the modeling to better resolve the kinetics of bimolecular recombinations to the R and T states. Without such a constraint, it was found that their kinetics tended to mix in the modeling because of the relative spectral similarity of their unliganded heme sites (*17*). This spectral constraint was implemented by comparing the T → R difference spectrum calculated from the model with the equilibrium difference spectrum measured by Perutz et al. (*50*). A penalty ρ proportional to the sum of squares of the deviation of the shape of the calculated spectrum from the Perutz spectrum was added to f, the total $f + \rho$ then being minimized as a function of the fitting parameters. (A proportionality factor assured that the penalty was roughly similar in magnitude to f. The results of the optimization were found to be insensitive to variations of this factor within an order of magnitude around values obeying the condition $f \approx \rho$.)

REFERENCES

1. Ackers, G. K., Doyle, M. L., Myers, D., and Daugherty, M. A. (1992) Molecular code for cooperativity in hemoglobin, *Science 255*, 54−63.
2. Monod, J., Wyman, J., and Changeux, J. P. (1965) On the nature of allosteric transitions: a plausible model, *J. Mol. Biol. 12*, 88−118.
3. Koshland, D. E., Nemethy, G., and Filmer, D. (1966) Comparison of experimental binding data and theoretical models in proteins containing subunits, *Biochemistry 5*, 365−385.
4. Ackers, G. K., Dalessio, P. J., Lew, G. H., Daugherty, M. A., and Holt, J. M. (2002) Single residue modification of only one dimer within the hemoglobin tetramer reveals autonomous dimer function, *Proc. Natl. Acad. Sci. U. S. A. 99*, 9777−9782.
5. Evans, M. G., and Polyanyi, M. (1938) Inertia and driving force of chemical reactions, *Trans. Faraday Soc. 34*, 11−24.
6. Eaton, W. A., Henry, E. R., and Hofrichter, J. (1991) Application of linear free energy relations to protein conformational changes: the quaternary structural change of hemoglobin, *Proc. Natl. Acad. Sci. U. S. A. 88*, 4472−4475.
7. Henry, E. R., Jones, C. M., Hofrichter, J., and Eaton, W. A. (1997) Can a two-state MWC allosteric model explain hemoglobin kinetics? *Biochemistry 36*, 6511−6528.
8. Sawicki, C. A., and Gibson, Q. H. (1976) Quaternary conformational changes in human hemoglobin studied by laser photolysis of carboxyhemoglobin, *J. Biol. Chem. 251*, 1533−1542.
9. Huang, Y., and Ackers, G. K. (1996) Transformation of cooperative free energies between ligation systems of hemoglobin: resolution of the carbon monoxide binding intermediates, *Biochemistry 35*, 704−718.
10. Goldbeck, R. A., Esquerra, R. M., Kliger, D. S., Holt, J. M., and Ackers, G. K. (2004) The molecular code for hemoglobin allostery revealed by linking the thermodynamics and kinetics of quaternary structural change. 2. Cooperative free energies of $(\alpha_{FeCO}\beta_{Fe})_2$ and $(\alpha_{Fe}\beta_{FeCO})_2$ T-state tetramers, *Biochemistry 43*, 12065−12080.
11. Goldbeck, R. A., and Kliger, D. S. (1993) Nanosecond time-resolved absorption and polarization dichroism spectroscopies, *Methods Enzymol. 226*, 147−177.
12. Alpert, B., El Mohsni, S., Lindqvist, L., and Tfibel, F. (1979) Transient effects in the nanosecond laser photolysis of carboxyhemoglobin: "cage" recombinations and spectral evolution of the protein, *Chem. Phys. Lett. 64*, 11−16.
13. Duddell, D. A., Morris, R. J., and Richards, J. T. (1979) Ultrafast recombination in nanosecond laser photolysis of carbonylhemoglobin, *J. Chem. Soc. Chem. Commun.* 75−76.
14. Friedman, J. M., and Lyons. K. B. (1980) Transient Raman study of CO-hemoprotein photolysis: origin of the quantum yield, *Nature 284*, 570−572.
15. Esquerra, R. M., Goldbeck, R. A., Reaney, S. H., Batchelder, A. M., Wen, Y., Lewis, J. W., and Kliger, D. S. (2000) Multiple geminate ligand recombinations in human hemoglobin, *Biophys. J. 78*, 3227−3239.
16. Friedman, J. M., Rousseau, D. L., and Ondrias, M. R. (1982) Time-resolved resonance Raman studies of hemoglobin, *Annu. Rev. Phys. Chem. 33*, 471−491.
17. Goldbeck, R. A., Paquette, S. J., Björling, S. C., and Kliger, D. S. (1996) Allosteric intermediates in hemoglobin. 2. Kinetic modeling of HbCO photolysis, *Biochemistry 35*, 8628−8639.
18. Jones, C. M., Ansari, A., Henry, E. R., Christoph, G. W., Hofrichter, J., and Eaton, W. A. (1992) Speed of intersubunit communication in proteins, *Biochemistry 31*, 6692−6702.
19. Rodgers, K. R., Su, C., Subramaniam, S., and Spiro, T. G. (1992) Hemoglobin R → T structural dynamics from simultaneous monitoring of tyrosine and tryptophan time-resolved UV resonance Raman signals, *J. Am. Chem. Soc. 114*, 3697−3709.
20. Jayaraman, V., Rodgers, K. R., Mukerji, I., and Spiro, T. G. (1995) Hemoglobin allostery: resonance Raman spectroscopy of kinetic intermediates, *Science 269*, 1843−1848.
21. Björling, S. C., Goldbeck, R. A., Paquette, S. J., Milder, S. J., and Kliger, D. S. (1996) Allosteric intermediates in hemoglobin. 1. Nanosecond time-resolved circular dichroism spectroscopy, *Biochemistry 35*, 8619−8627.
22. Goldbeck, R. A., Esquerra, R. M., and Kliger, D. S. (2002) Hydrogen bonding to Trp β37 is the first step in a compound pathway for hemoglobin allostery, *J. Am. Chem. Soc. 124*, 7646−7647.
23. Hofrichter, J., Henry, E. R., Szabo, A., Murray, L. P., Ansari, A., Jones, C. M., Coletta, M., Falcioni, G., Brunori, M., and Eaton, W. A. (1991) Dynamics of the quaternary conformational change in trout hemoglobin, *Biochemistry 30*, 6583−6598.
24. Shulman, R. G., Hopfield, J. J., and Ogawa, S. (1975) Allosteric interpretation of hemoglobin properties, *Quart. Rev. Biophys. 8*, 325−420.
25. Dickerson, R. E., and Geis, I. (1983) *Hemoglobin*: *Structure*, *Function*, *Evolution*, *and Pathology*, Benjamin/Cummings, Menlo Park.
26. Robert, C. H., Fall, L., and Gill, S. J. (1988) Linkage of organic phosphates to oxygen binding in human hemoglobin at high concentrations, *Biochemistry 27*, 6835−6843.
27. Imaizumi, K., Imai, K., and Tyuma, I. (1979) The linkage between the four-step binding of oxygen and the binding of heterotropic anionic ligands in hemoglobin, *J. Biochem.* (*Tokyo*) *86*, 1829−1840.
28. Gray, R. D., and Gibson, Q. H. (1971) The binding of carbon monoxide to α and β chains in tetrameric mammalian hemoglobin, *J. Biol. Chem. 246*, 5176−5178.
29. Jameson, G. B., and Ibers, J. A. (1994) Biological and Synthetic Dioxygen Carriers, in *Bioinorganic Chemistry* (Bertini, I., Gray, H. B., Lippard, S. J., and Valentine, J. S., Eds.) pp 167−252, University Science Books, Mill Valley.
30. Marden, M. C., Kister, J., Bohn, B., and Poyart, C. (1988) T-state hemoglobin with four ligands bound, *Biochemistry 27*, 1659−1664.
31. Khan, I., Dantsker, D., Samuni, U., Friedman, A. J., Bonaventura, C., Manjula, B., Acharya, S. A., and Friedman, J. M. (2001) β93 modified hemoglobin: Kinetic and conformational consequences, *Biochemistry 40*, 7581−7592.
32. Tsuneshige, A., Park, S., and Yonetani, T. (2002) Heterotropic effectors control the hemoglobin function by interacting with its T and R state: a new view on the principle of allostery, *Biophys. Chem. 98*, 49−63.
33. Peterson, E. S., Shinder, R., Khan, I., Juczszak, L., Wang, J., Manjula, B., Acharya, S. A., Bonaventura, C., and Friedman, J. M. (2004) Domain-specific effector interactions within the central cavity of human adult hemoglobin in solution and in porous sol−gel matrices: Evidence for long-range communication pathways, *Biochemistry 43*, 4832−4843.
34. Noble, R. W., Hui, H. L., Kwiatkowski, L. D., Paily, P., DeYoung, A., Wierzba, A., and Colby, J. E. (2001) Mutational effects at the subunit interfaces of human hemoglobin: Evidence for a unique sensitivity of the T quaternary state to changes in the hinge region of the $\alpha_1\beta_2$ interface, *Biochemistry 40*, 12357−12368.
35. Szabo, A. (1978) Kinetics of hemoglobin and transition state theory, *Proc. Natl. Acad. Sci. U. S. A. 75*, 2108−2111.
36. Lavalette, D., Tetreau, C., Mispelter, J., Momenteau, M., and Lhoste, J.-M. (1984) Linear free-energy relationships in binding of oxygen and carbon monoxide with heme model compounds and heme proteins, *Eur. J. Biochem. 145*, 555−565.
37. Zhao, M., Jiang, J., Greene, M., Andracki, M. E., Fowler, S. A., Walder, J. A., and Ferrone, F. A. (1993) Allosteric kinetics and equilibria of triligated, cross-linked hemoglobin, *Biophys. J. 64*, 1520−1532.

38. Goldbeck, R. A., Paquette, S. J., and Kliger, D. S. (2001) The effect of water on the rate of conformational change in protein allostery, *Biophys. J. 81*, 2919−2934.
39. Shulman, R. G., Ogawa, S., and Mayer, A. (1982) The Two-State Model of Hemoglobin: Hb Kansas as a Model for the Low-Affinity State, in *Hemoglobin and Oxygen Binding* (Ho, C., Ed.) pp 205−209, Elsevier, New York.
40. Perutz, M. F. (1970) Stereochemistry of cooperative effects in haemoglobin, *Nature 228*, 726−739.
41. Paquette, S. J. (1999) *Dynamics of Human Hemoglobin in Poly(ethylene glycol)−Water Solutions: Kinetic Effects of PEG on the Allosteric Transition and CO−Rebinding Reactions*, Ph. D. dissertation, University of California, Santa Cruz.
42. Parkhurst, L. J. (1979) Hemoglobin and myoglobin ligand kinetics, *Annu. Rev. Phys. Chem. 30*, 503−546.
43. Hofrichter, J., Henry, E. R., Sommer, J. H., Deutsch, R., Ikeda-Saito, M., Yonetani, T., and Eaton, W. A. (1985) Nanosecond optical spectra of iron−cobalt hybrid hemoglobins: geminate recombination, conformational changes, and intersubunit communication, *Biochemistry 24*, 2667−2679.
44. Bandyopadhyay, D., Magde, D., Traylor, T. G., and Sharma, V. S. (1992) Quaternary structure and geminate recombination in hemoglobin: flow-flash studies on $\alpha_2^{CO}\beta_2$ and $\alpha_2\beta_2^{CO}$, *Biophys. J. 63*, 673−681.
45. Mozzarelli, A, Rivetti, C., Rossi, G. L., Henry, E. R., and Eaton, W. A. (1991) Crystals of haemoglobin with the T quaternary structure bind oxygen noncooperatively with no Bohr effect, *Nature 351*, 416−419.
46. Rivetti, C., Mozzarelli, A., Rossi, G. L., Henry, E. R., and Eaton, W. A. (1993) Oxygen binding by single crystals of hemoglobin, *Biochemistry 32*, 2888−2906.
47. Samuni, U., Juszczak, L., Dantsker, D., Khan, I., Friedman, A. J., Pérez-González-de-Apodaca, Bruno, S., Hui, H. L., Colby, J. E., Karasik, E., Kwiatkowski, L. D., Mozzarelli, A., Noble, R., and Friedman, J. M. (2003) Functional and spectroscopic characterization of half-liganded iron−zinc hybrid hemoglobin: Evidence for conformational plasticity within the T state, *Biochemistry 42*, 8272−8288.
48. Henry, E. R., Bettati, S., Hofrichter, J., and Eaton, W. A. (2002) A tertiary two-state allosteric model for hemoglobin, *Biophys. Chem. 98*, 149−164.
49. Goldbeck, R. A., and Kliger, D. S. (2001) Transient Kinetic Studies, in *Encyclopedia of Chemical Physics and Physical Chemistry* (Moore, J. H., and Spencer, N. D., Eds.) pp 2637−2656, IOP, Bristol.
50. Perutz, M. F., Ladner, J. E., Simon, S. R., and Ho, C. (1974) Influence of globin structure on the state of the heme. I. Human deoxyhemoglobin, *Biochemistry 13*, 2163−2172.

BI049393V